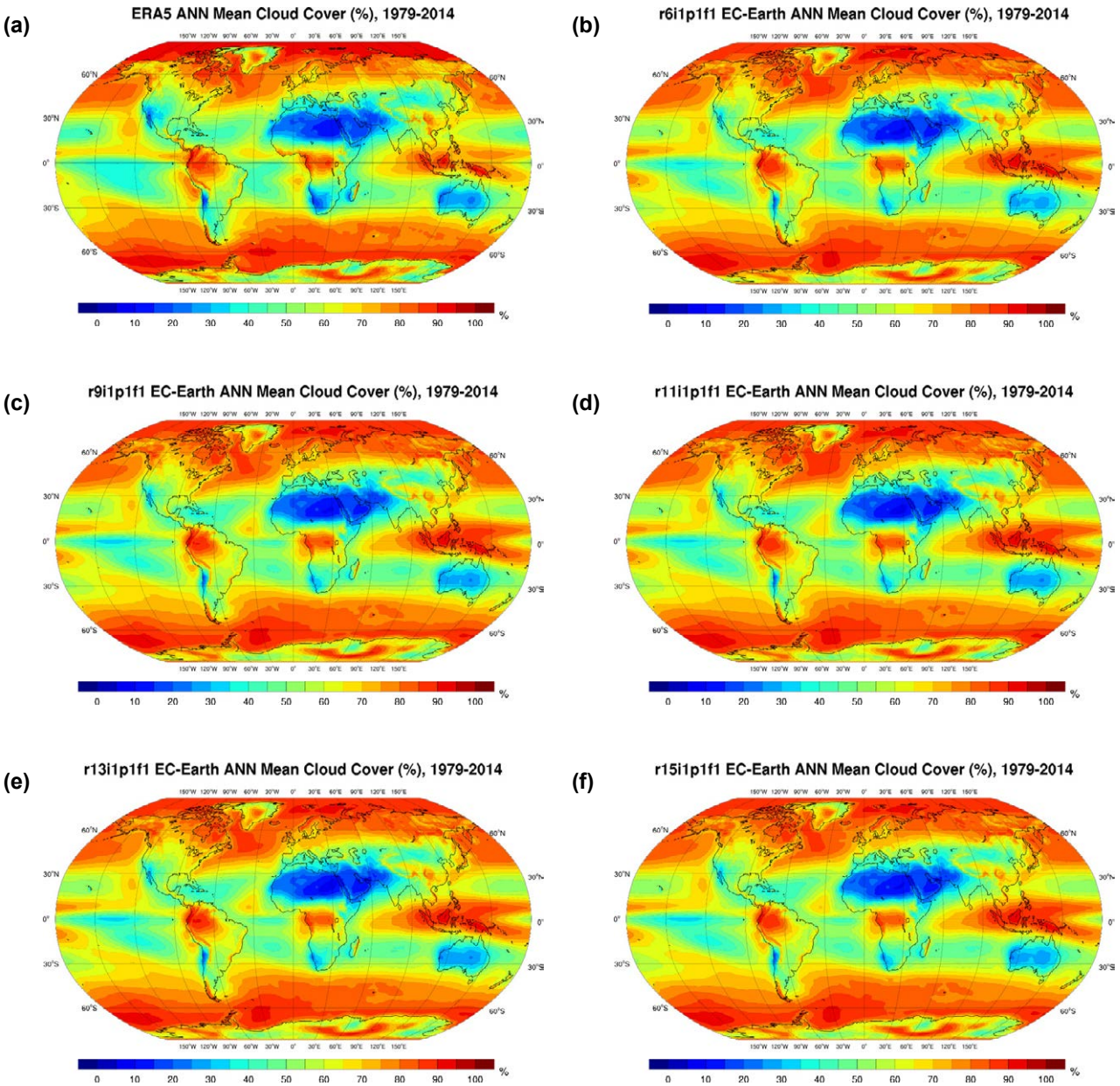

Figure 2.37. Annual mean cloud cover (%), 1979–2014: (a) ERA5 reanalysis, (b) EC-Earth r6i1p1f1, (c) EC-Earth r9i1p1f1, (d) EC-Earth r11i1p1f1, (e) EC-Earth r13i1p1f1 and (f) EC-Earth r15i1p1f1.

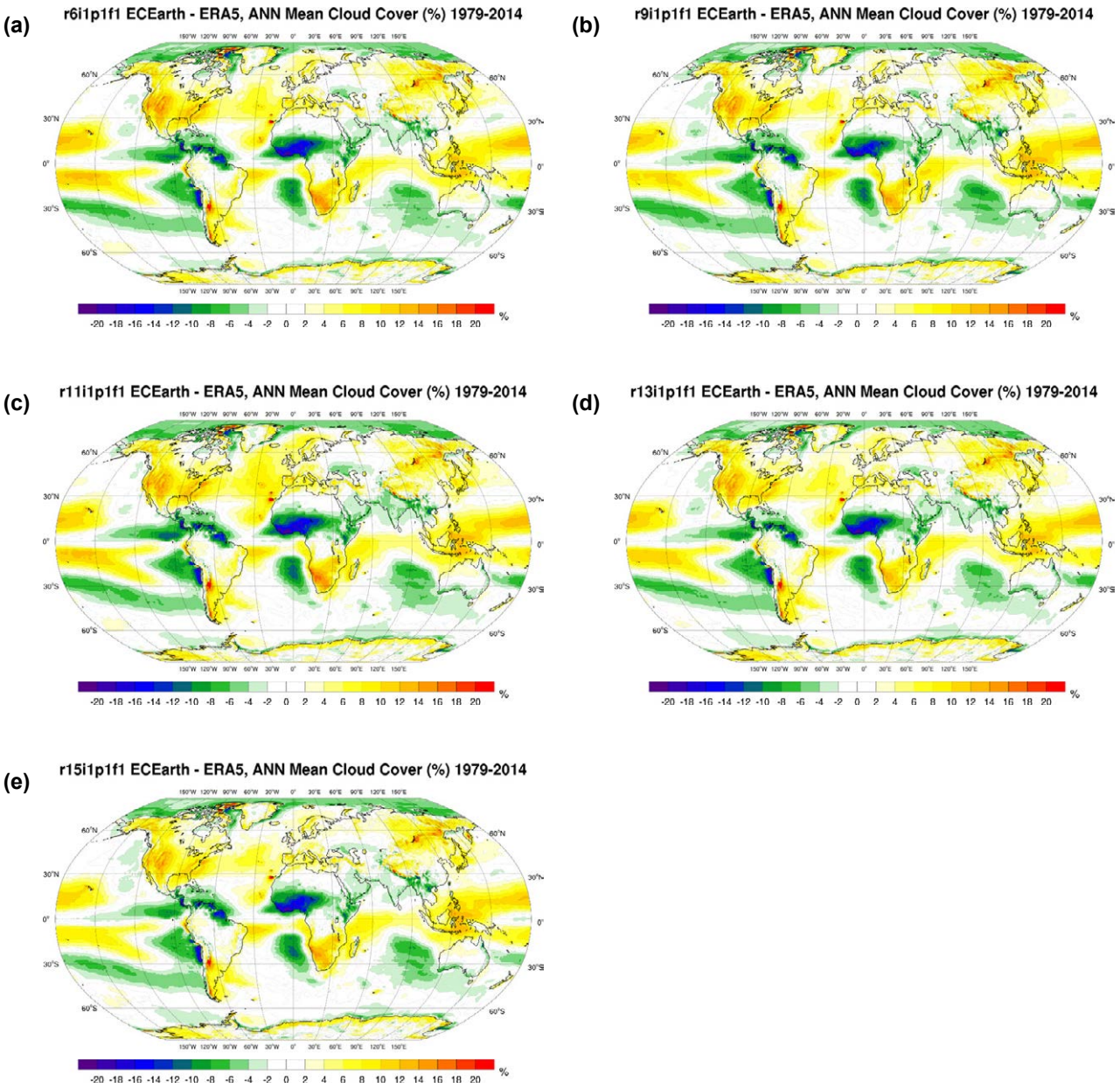

Figure 2.38. EC-Earth annual cloud cover bias (%), 1979–2014 (ERA5 reanalysis minus EC-Earth): (a) EC-Earth r6i1p1f1, (b) EC-Earth r9i1p1f1, (c) EC-Earth r11i1p1f1, (d) EC-Earth r13i1p1f1 and (e) EC-Earth r15i1p1f1.

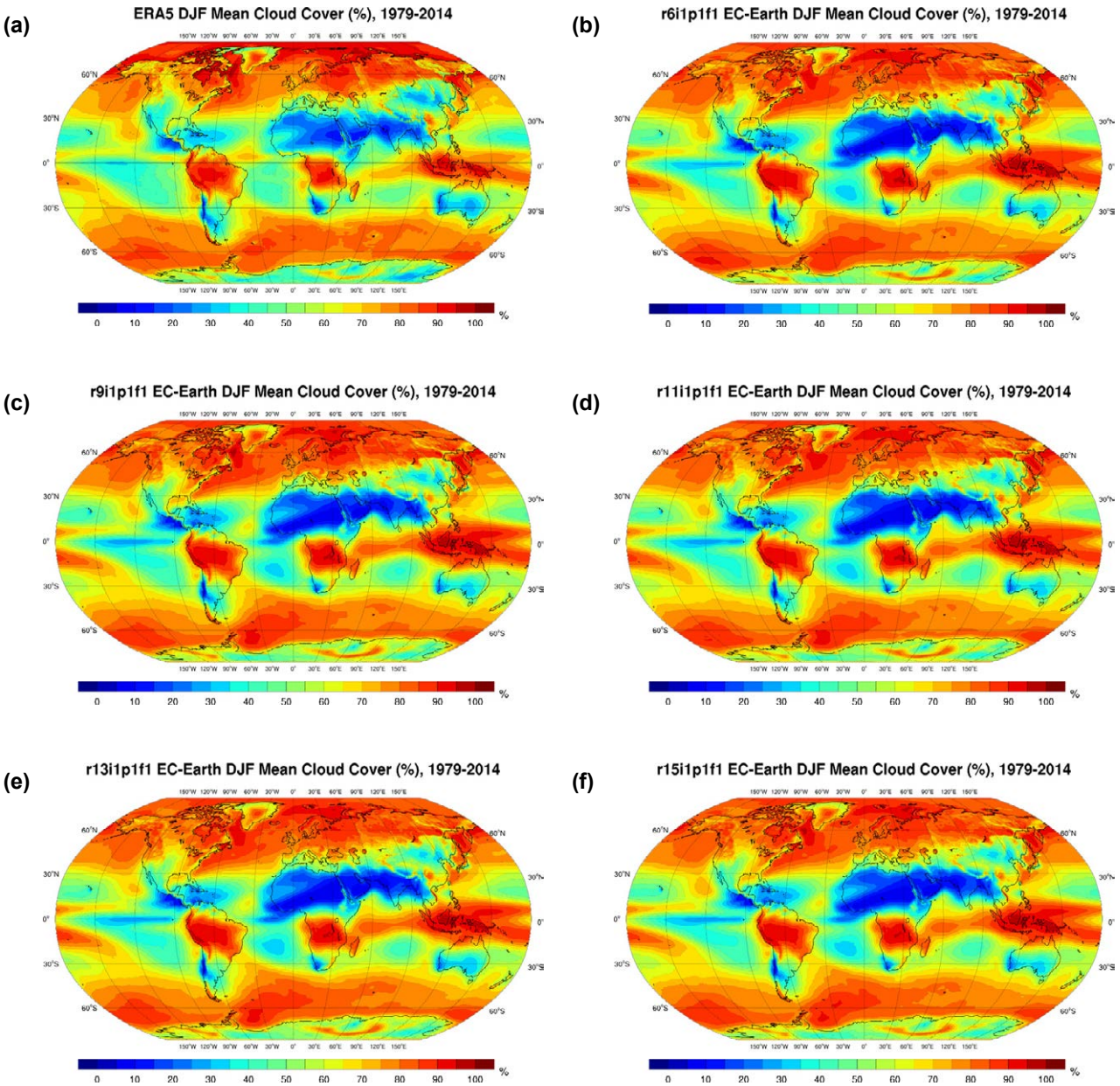

Figure 2.39. Mean cloud cover (%) for DJF, 1979–2014: (a) ERA5 reanalysis, (b) EC-Earth r6i1p1f1, (c) EC-Earth r9i1p1f1, (d) EC-Earth r11i1p1f1, (e) EC-Earth r13i1p1f1 and (f) EC-Earth r15i1p1f1.

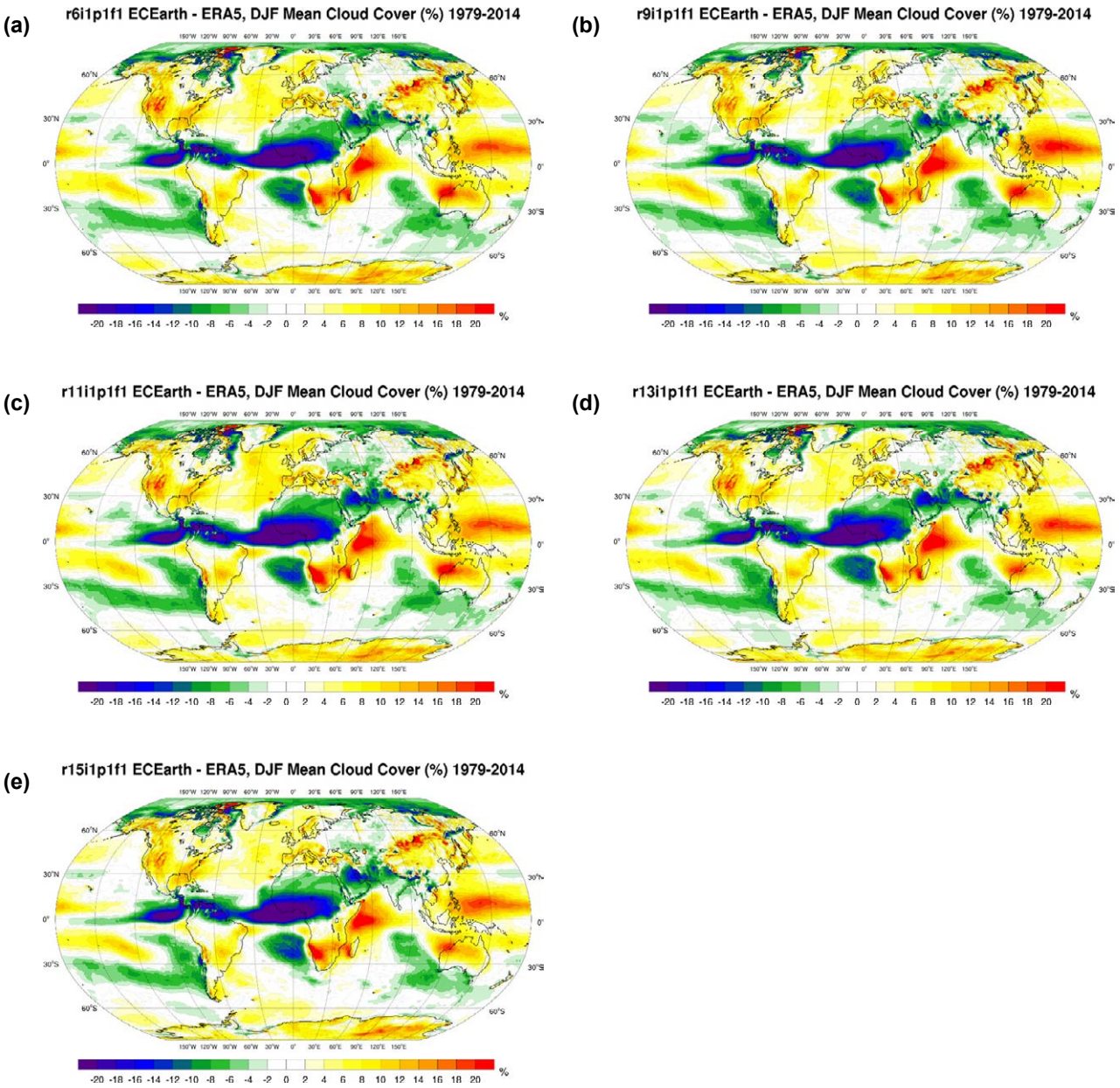

Figure 2.40. EC-Earth cloud cover bias (%) for DJF, 1979–2014 (ERA5 reanalysis minus EC-Earth): (a) EC-Earth r6i1p1f1, (b) EC-Earth r9i1p1f1, (c) EC-Earth r11i1p1f1, (d) EC-Earth r13i1p1f1 and (e) EC-Earth r15i1p1f1.

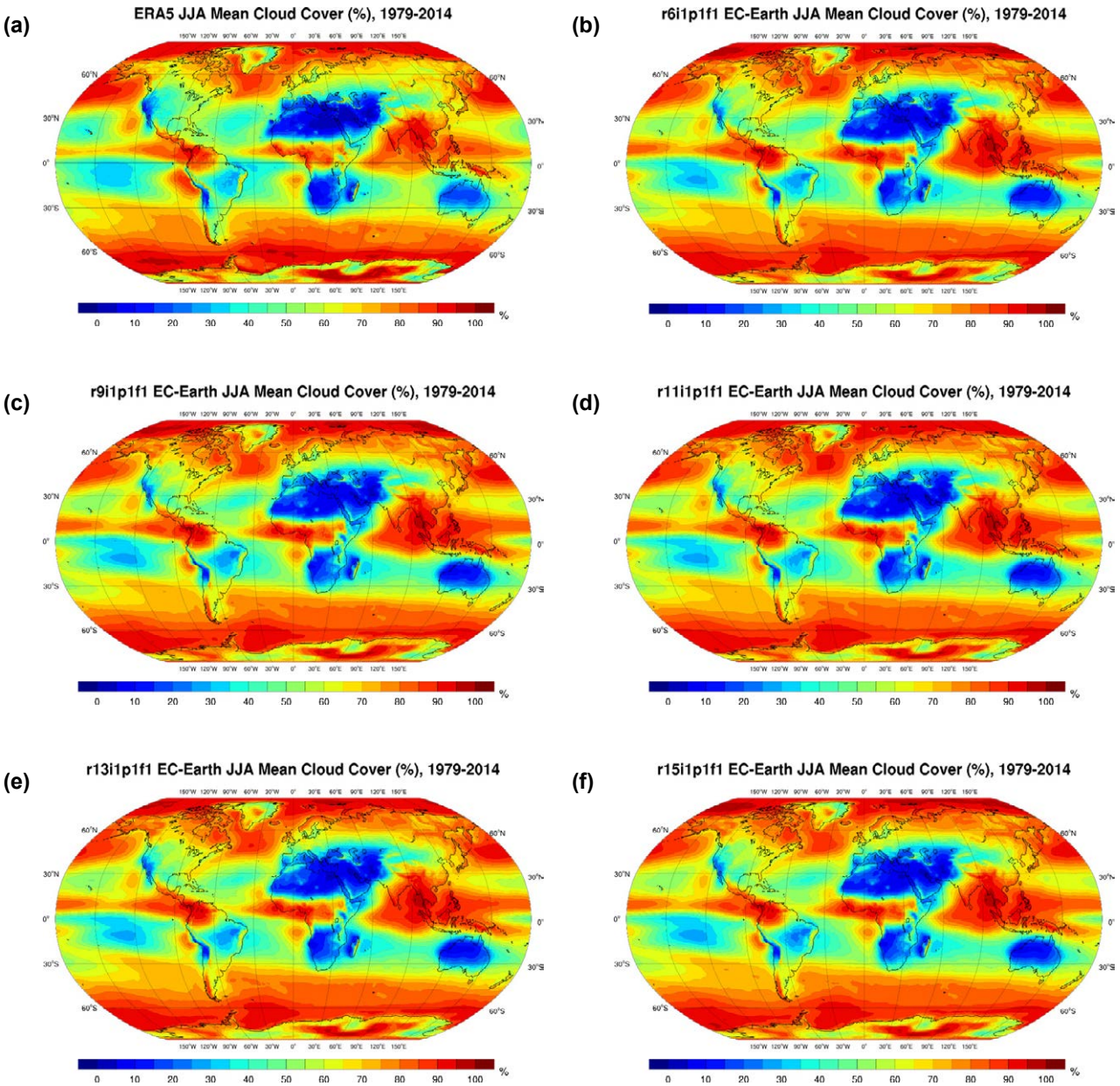

Figure 2.41. Mean cloud cover (%) for JJA, 1979–2014: (a) ERA5 reanalysis, (b) EC-Earth r6i1p1f1, (c) EC-Earth r9i1p1f1, (d) EC-Earth r11i1p1f1, (e) EC-Earth r13i1p1f1 and (f) EC-Earth r15i1p1f1.

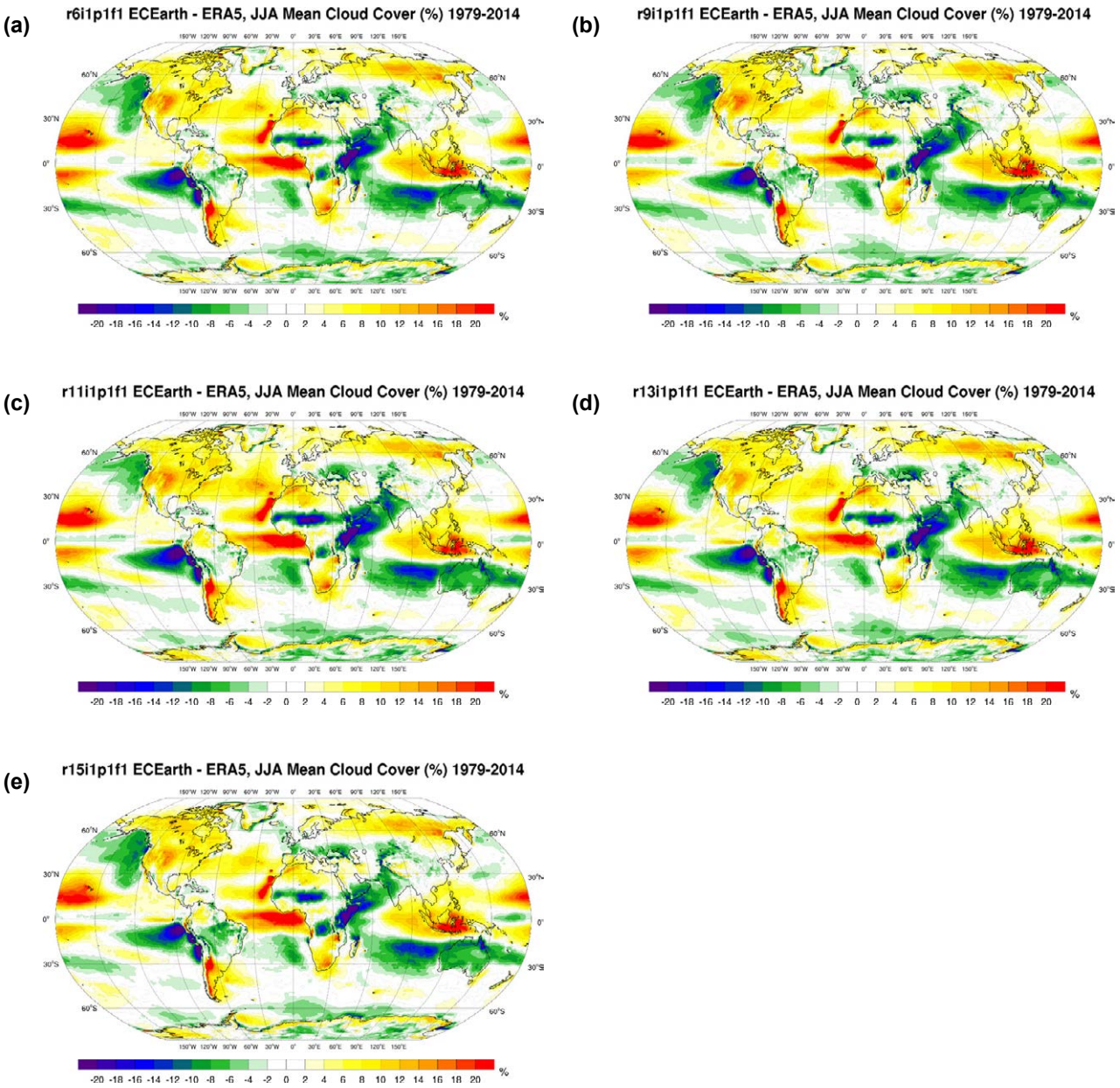

Figure 2.42. EC-Earth cloud cover bias (%) for JJA, 1979–2014 (ERA5 reanalysis minus EC-Earth): (a) EC-Earth r6i1p1f1, (b) EC-Earth r9i1p1f1, (c) EC-Earth r11i1p1f1, (d) EC-Earth r13i1p1f1 and (e) EC-Earth r15i1p1f1.

The annual and seasonal overall global cloud cover bias and MAE statistics relative to ERA5 data (1979–2014) for each of the five ensemble members are presented in Table 2.8. The bias statistics are all positive, ranging from 0.95% (DJF, r15i1p1f1) to 1.55% (SON, r11i1p1f1). The MAE statistics range from 3.91% (annual, r15i1p1f1) to 6.36% (MAM, r11i1p1f1).

The ERA5 and EC-Earth mean global annual total cloud cover time series (1979–2014), presented in Figure 2.43a, demonstrate good agreement. However, all EC-Earth ensemble members exhibit a slight overestimation of cloud cover of ~1.5% relative to ERA5 data. Figure 2.43b shows the annual anomalies with respect to the 1981–2010 mean; all ERA5 and EC-Earth annual values are within the range of ±0.6%.

Table 2.8. Mean global annual and seasonal cloud cover bias and MAE (%) for each of the five EC-Earth ensemble members[a]

Time period	r6i1p1f1		r9i1p1f1		r11i1p1f1		r13i1p1f1		r15i1p1f1	
	Bias	MAE	Bias	MAE	Bias	MAE	Bias	MAE	Bias	MAE
Annual	1.25	4.03	1.12	4.0	1.27	4.24	1.21	4.02	1.12	3.91
DJF	1.07	5.74	1.01	5.75	1.0	6.03	1.03	5.82	0.95	5.60
MAM	1.17	6.08	0.97	6.22	1.11	6.36	1.10	6.08	1.01	6.05
JJA	1.31	5.12	1.15	5.12	1.43	5.32	1.27	5.21	1.19	5.04
SON	1.48	4.53	1.36	4.61	1.55	4.68	1.43	4.55	1.32	4.42

[a]In each case the model data are compared with ERA5 reanalysis data for the period 1979–2014.

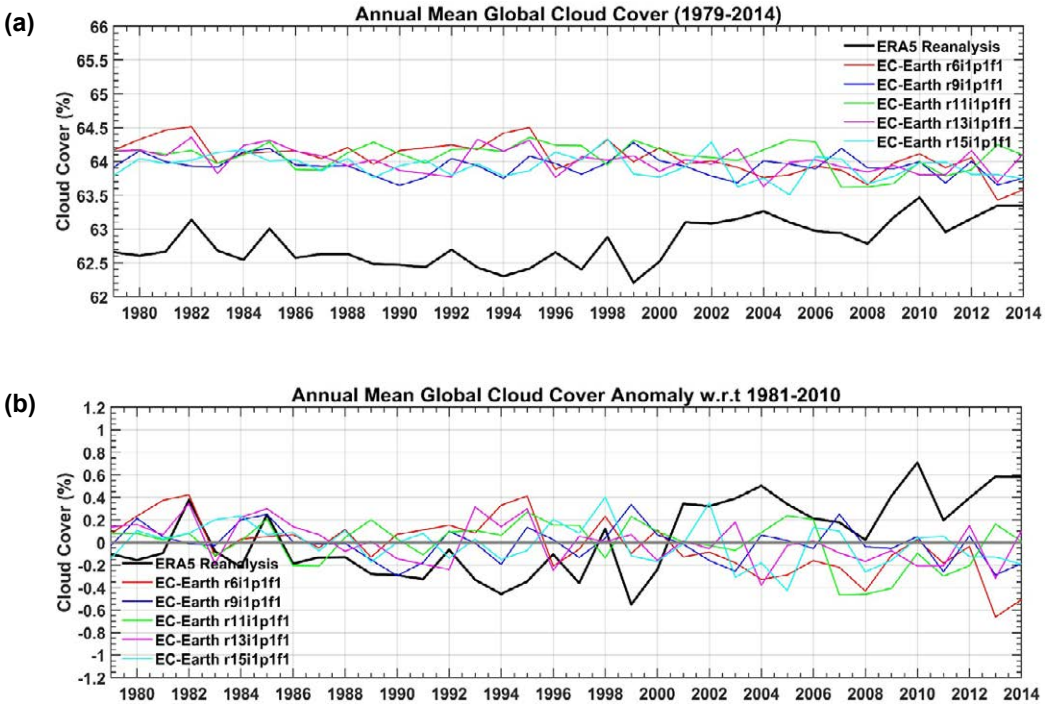

Figure 2.43. Comparison of EC-Earth ensemble members with ERA5 reanalysis data for the period 1979–2014: (a) cloud cover and (b) cloud cover anomalies with respect to the 30-year period 1981–2010.

2.3.6 Snowfall validations

Figure 2.44 presents the annual mean snowfall (mm/day) for ERA5 and the five EC-Earth ensemble members for the period 1979–2014. The EC-Earth ensemble members perform well relative to ERA5 data, showing similar spatial magnitudes and spatial distributions of snowfall. Figure 2.45 demonstrates that the differences relative to ERA5 data are similar for all EC-Earth ensemble members – an underestimation over the Southern and Arctic Oceans and a slight overestimation over Antarctica. A slight overestimation is also noted over the north-west Atlantic for ensemble members r6i1p1f1 and r11i1p1f1. Snowfall validations for DJF (Figures 2.46 and 2.47) show a similar (but enhanced) signal to the annual validations. In addition, a negative bias is noted over much of Europe and Russia. Snowfall validations for JJA (Figures 2.48 and 2.49) show a positive bias over Antarctica and a negative bias over the Southern Hemisphere oceans.

The global annual snowfall anomalies with respect to the 1981–2010 mean, presented in Figure 2.50, demonstrate good agreement between the EC-Earth ensemble members and ERA5; all ERA5 and EC-Earth annual values are within the range of –6% to 4%.

2.3.7 Sea surface temperature validations

Figure 2.51 shows the ERA5 and EC-Earth mean annual SST for 1979–2014. All EC-Earth ensemble members accurately capture the magnitude and spatial characteristics of SST. Figure 2.52 demonstrates that the differences relative to ERA5 data are similar for all EC-Earth ensemble members, with a warm bias over most regions, in particular the Southern Hemisphere oceans. A cold bias is noted over the North Atlantic, the magnitude of which varies between ensemble members; the largest cold bias is noted for ensemble member r11i1p1f1 (Figure 2.52c). SST validations for DJF (Figures 2.53 and 2.54) and JJA (Figures 2.55 and 2.56) exhibit a similar signal to the annual validations.

In order to quantify the EC-Earth cold bias over the North Atlantic, the mean and minimum bias values were calculated over the area 40–60°N, 25–55°W. The results, presented in Table 2.9, show that the cold anomaly exists for all ensemble members and all seasons, with the largest biases noted for r11i1p1f1.

The annual and seasonal overall global bias and MAE statistics relative to ERA5 data (1979–2014) for each of the five ensemble members are presented in Table 2.10. The bias statistics are all positive, ranging from 0.67°C (SON, r11i1p1f1) to 1.32°C (DJF, r9i1p1f1). The MAE statistics range from 1.03°C (SON, r6i1p1f1) to 1.63°C (MAM, r11i1p1f1).

The ERA5 and EC-Earth mean global annual SST time series (1979–2014), presented in Figure 2.57a, show that all EC-Earth ensemble members exhibit an overestimation of SST of ~1°C. Figure 2.57b shows the annual SST anomalies with respect to the 1981–2010 mean; there is a slight overestimation of the EC-Earth SST rise during the later years.

2.3.8 Sea ice fraction validations

The Northern Hemisphere mean annual sea ice fraction (1979–2014) for ERA5 and each of the five EC-Earth ensemble members is presented in Figure 2.58. The green line shows the 50% contour line. All EC-Earth ensemble members are similar to ERA5 but show an overestimation of the extent of the sea ice. The Northern Hemisphere sea ice fractions for March and September are presented in Figures 2.59 and 2.60, respectively. Again, all ensemble members are similar to ERA5 but show a slight overestimation of the extent of the sea ice. Similarly, the Southern Hemisphere sea ice fraction is presented in Figure 2.61 (annual), Figure 2.62 (March) and Figure 2.63 (September). In the Southern Hemisphere, all EC-Earth ensemble members underestimate sea ice extent (and fraction; see below), particularly during March.

Figure 2.64 presents the ERA5 and EC-Earth Northern Hemisphere sea ice fraction time series (1979–2014) over the full year and for March and September. A close agreement is noted for all EC-Earth ensemble members relative to ERA5 data, with EC-Earth performing best during September and over the full year. Figure 2.65 shows the sea ice fraction anomalies with respect to the 1981–2010 mean over the full year and for March and September; all EC-Earth ensemble members accurately resolve the downwards trend in Northern Hemisphere sea ice fraction.

Figure 2.66 presents the ERA5 and EC-Earth Southern Hemisphere sea ice fraction time series (1979–2014) over the full year and for March and September. An underestimation is noted for all EC-Earth ensemble members relative to ERA5 data. Figure 2.67 shows the annual sea ice fraction anomalies with respect to the 1981–2010 mean over the full year and for March and September; the EC-Earth anomalies are in close agreement with ERA5.

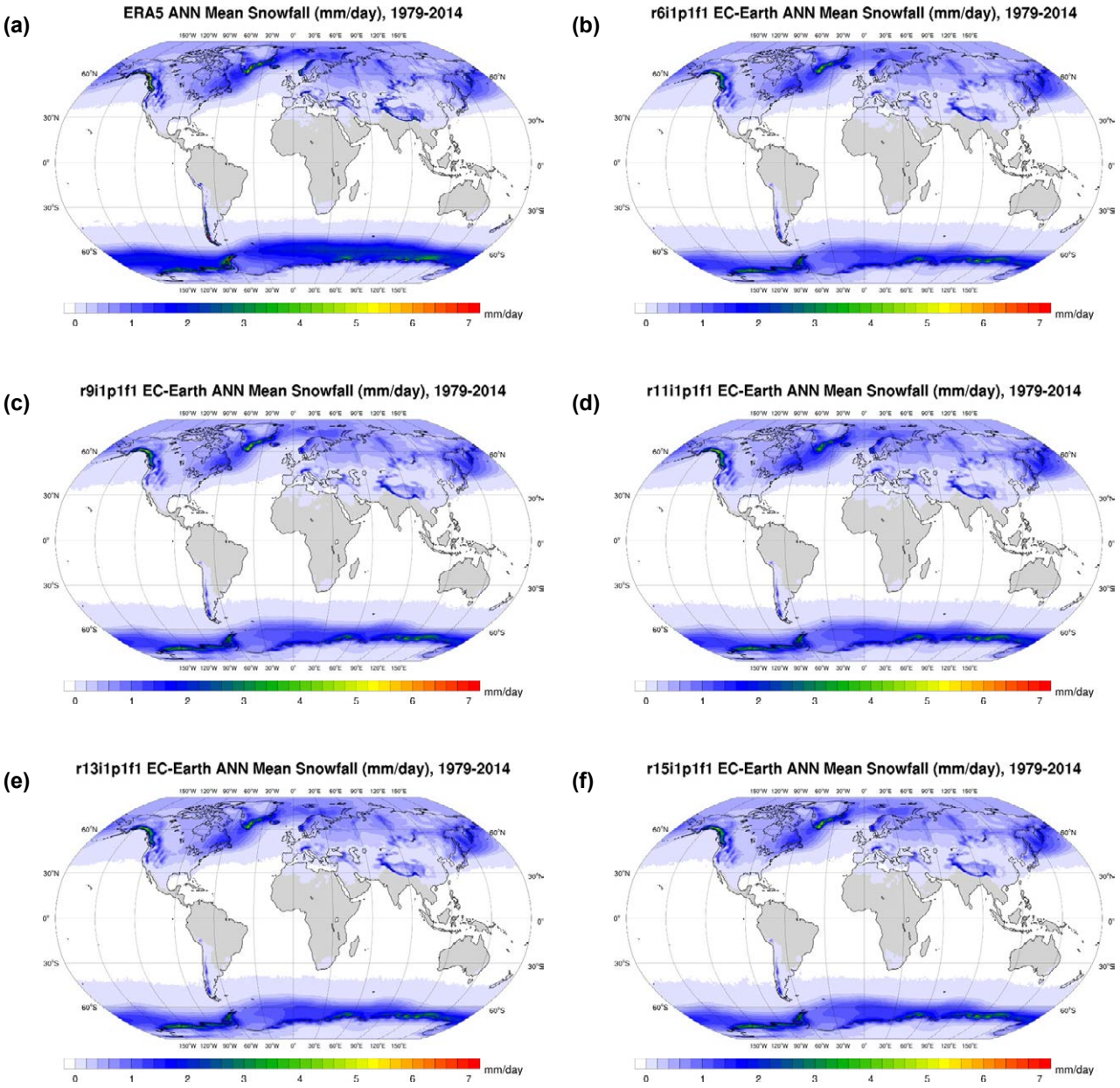

Figure 2.44. Annual mean daily snowfall (mm/day), 1979–2014: (a) ERA5 reanalysis, (b) EC-Earth r6i1p1f1, (c) EC-Earth r9i1p1f1, (d) EC-Earth r11i1p1f1, (e) EC-Earth r13i1p1f1 and (f) EC-Earth r15i1p1f1.

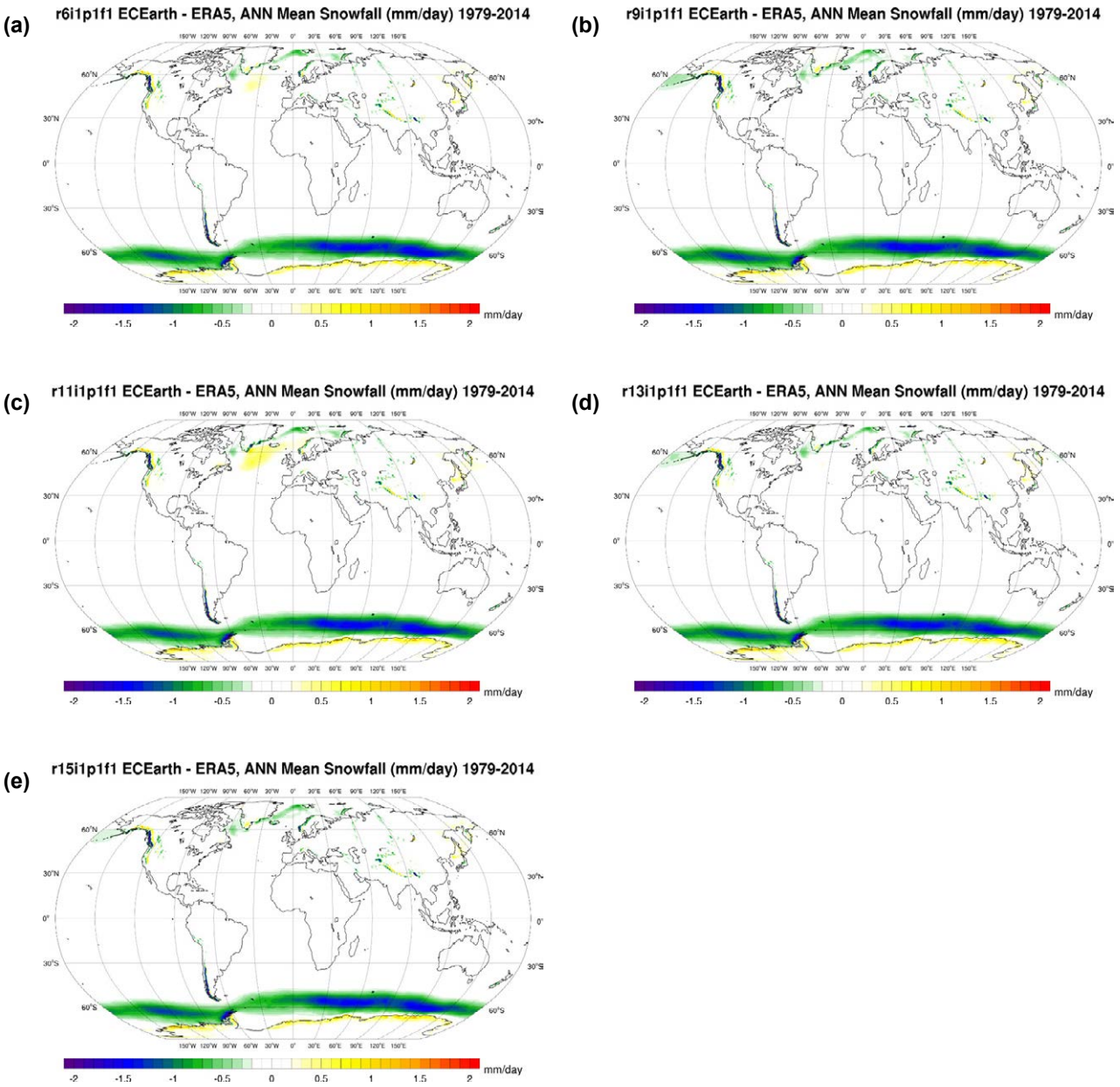

Figure 2.45. EC-Earth annual mean daily snowfall bias (mm/day), 1979–2014 (ERA5 reanalysis minus EC-Earth): (a) EC-Earth r6i1p1f1, (b) EC-Earth r9i1p1f1, (c) EC-Earth r11i1p1f1, (d) EC-Earth r13i1p1f1 and (e) EC-Earth r15i1p1f1.

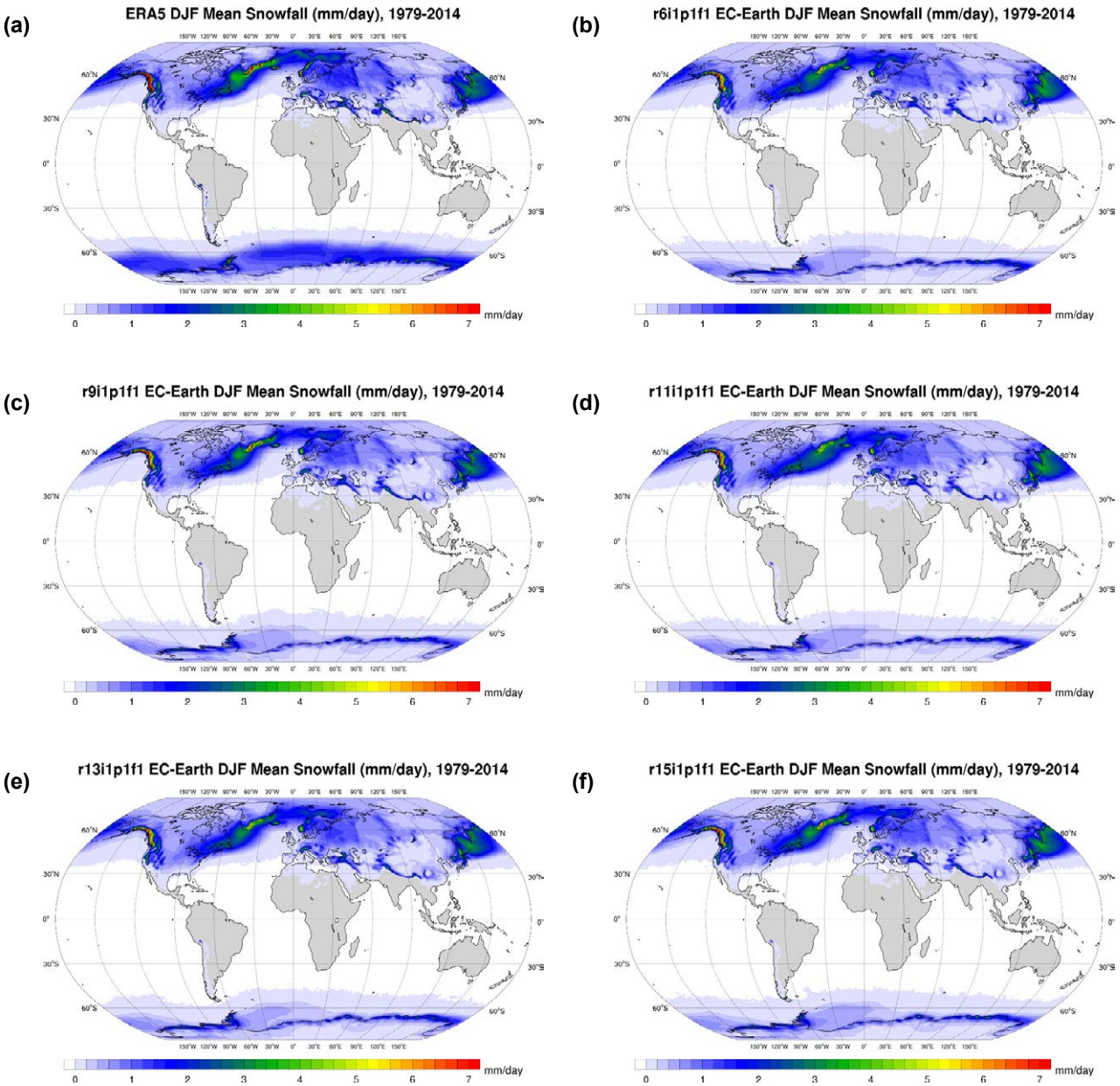

Figure 2.46. Mean daily snowfall (mm/day) for DJF, 1979–2014: (a) ERA5 reanalysis, (b) EC-Earth r6i1p1f1, (c) EC-Earth r9i1p1f1, (d) EC-Earth r11i1p1f1, (e) EC-Earth r13i1p1f1 and (f) EC-Earth r15i1p1f1.

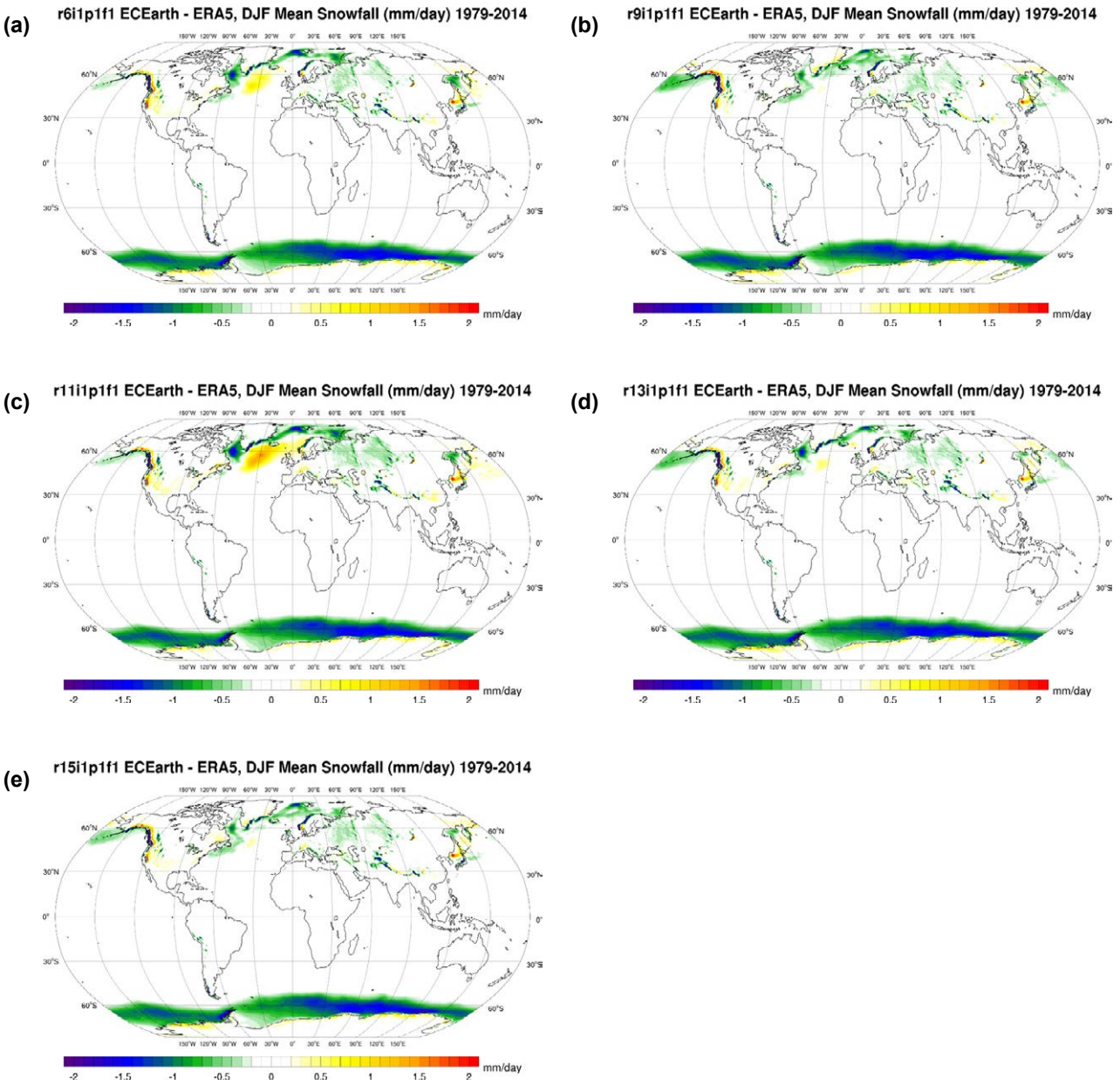

Figure 2.47. EC-Earth mean daily snowfall bias (mm/day) for DJF, 1979–2014 (ERA5 reanalysis minus EC-Earth): (a) EC-Earth r6i1p1f1, (b) EC-Earth r9i1p1f1, (c) EC-Earth r11i1p1f1, (d) EC-Earth r13i1p1f1 and (e) EC-Earth r15i1p1f1.

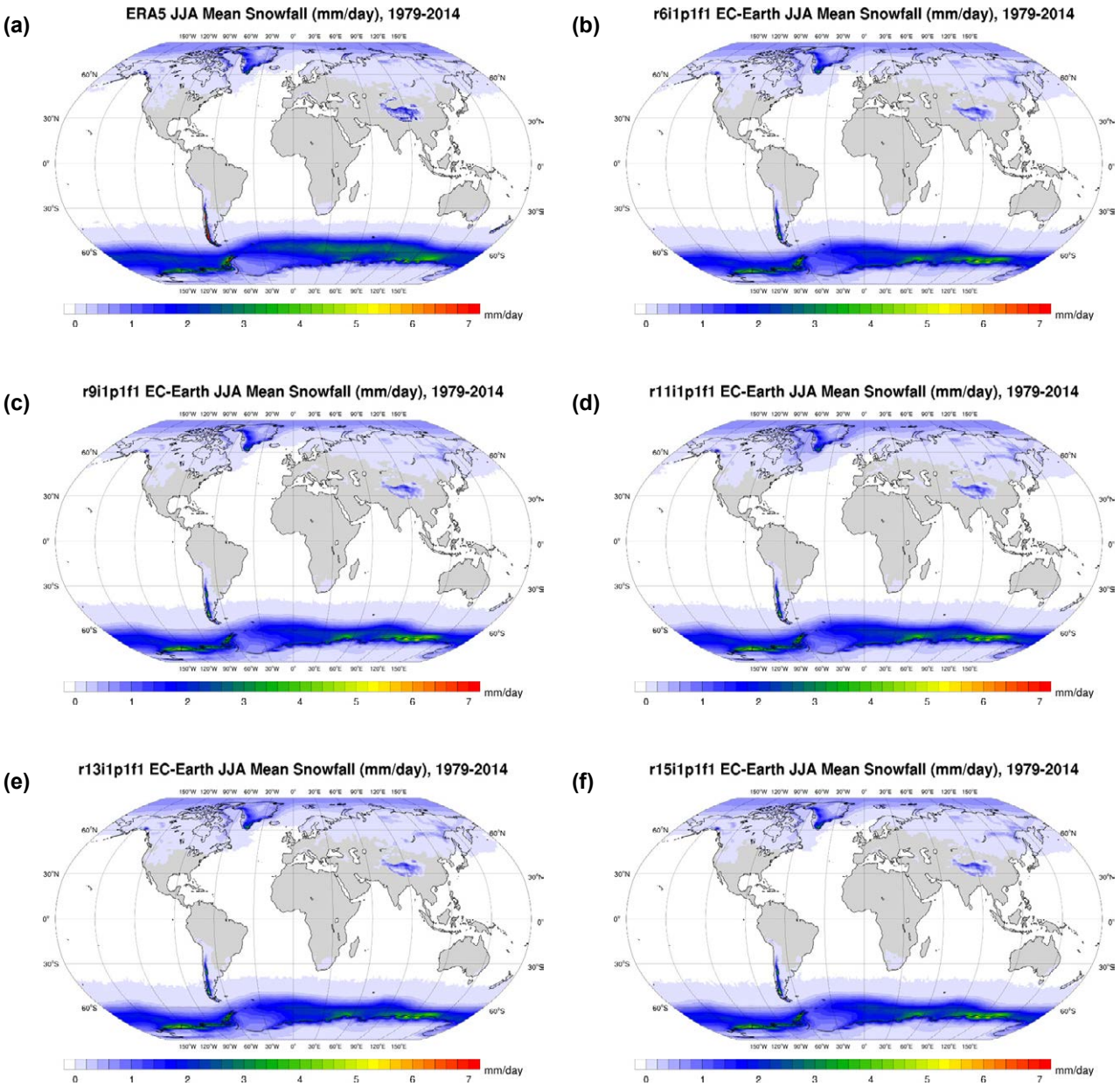

Figure 2.48. Mean daily snowfall (mm/day) for JJA, 1979–2014: (a) ERA5 reanalysis, (b) EC-Earth r6i1p1f1, (c) EC-Earth r9i1p1f1, (d) EC-Earth r11i1p1f1, (e) EC-Earth r13i1p1f1 and (f) EC-Earth r15i1p1f1.

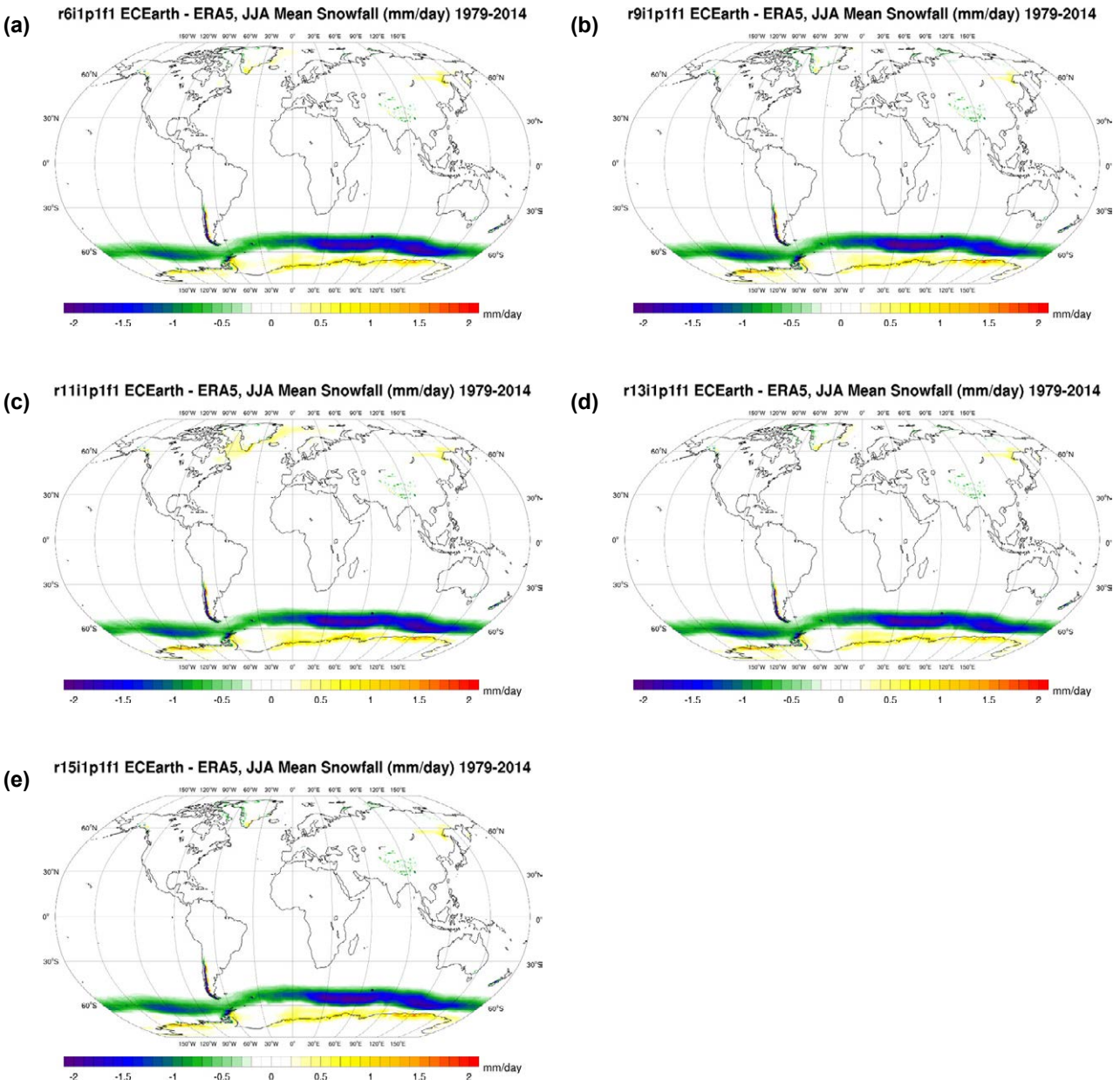

Figure 2.49. EC-Earth mean daily snowfall bias (mm/day) for JJA, 1979–2014 (ERA5 reanalysis minus EC-Earth): (a) EC-Earth r6i1p1f1, (b) EC-Earth r9i1p1f1, (c) EC-Earth r11i1p1f1, (d) EC-Earth r13i1p1f1 and (e) EC-Earth r15i1p1f1.

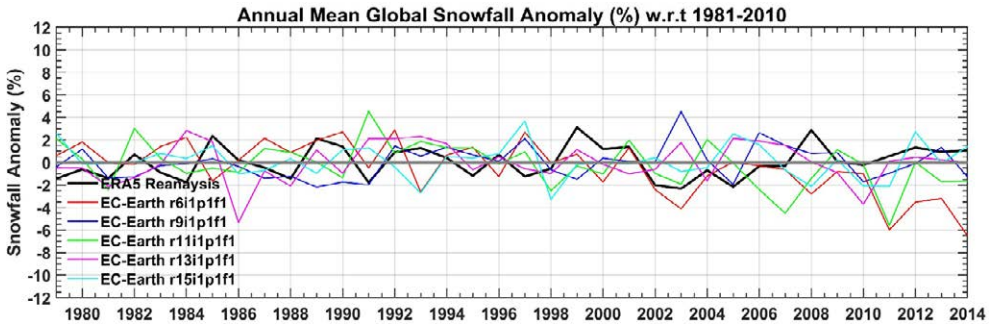

Figure 2.50. Comparison of EC-Earth ensemble members with ERA5 reanalysis data for the period 1979–2014: global annual snowfall anomalies (%) with respect to the 30-year period, 1981–2010.

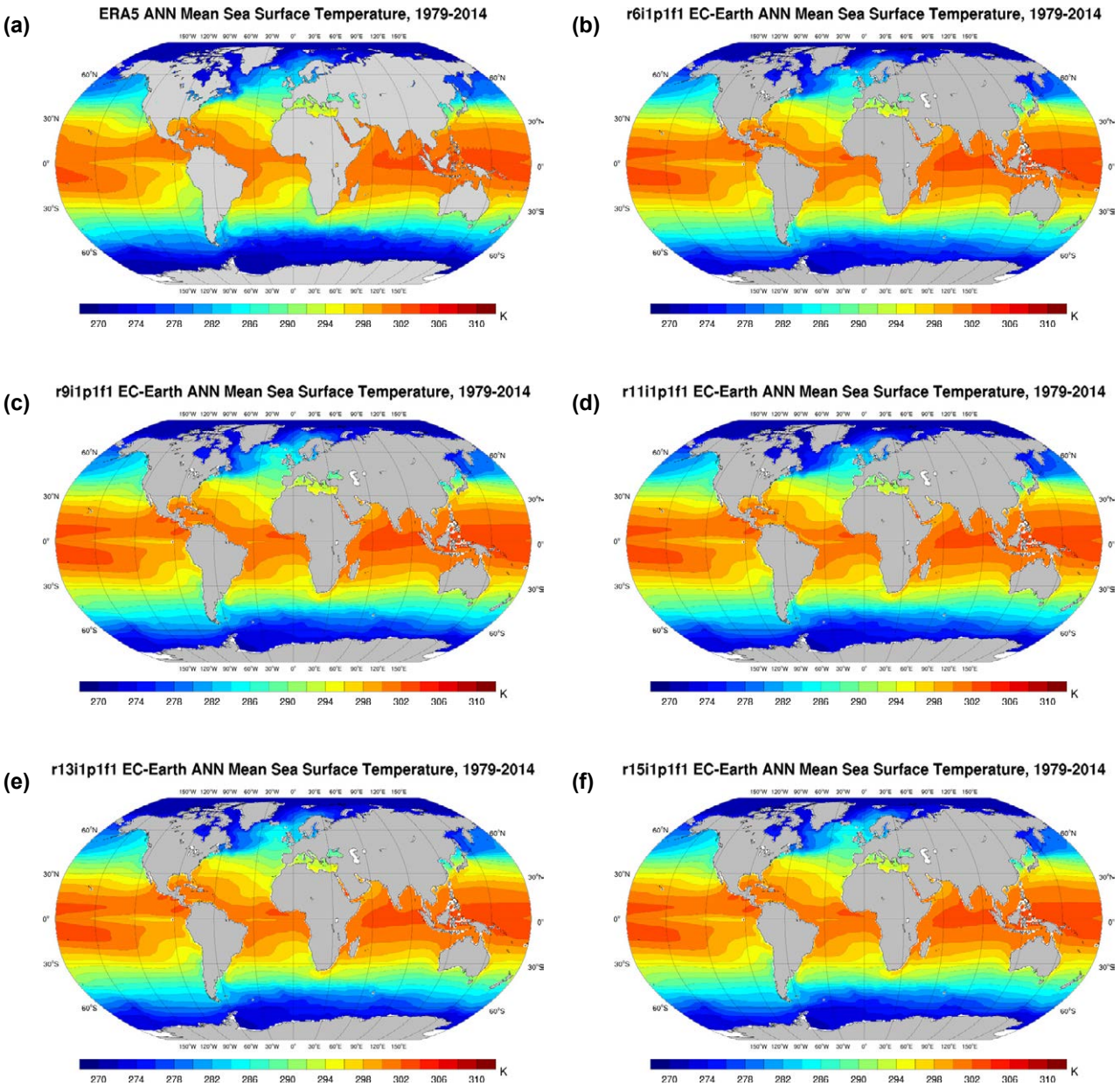

Figure 2.51. Annual mean SST (K), 1979–2014: (a) ERA5 reanalysis, (b) EC-Earth r6i1p1f1, (c) EC-Earth r9i1p1f1, (d) EC-Earth r11i1p1f1, (e) EC-Earth r13i1p1f1 and (f) EC-Earth r15i1p1f1.

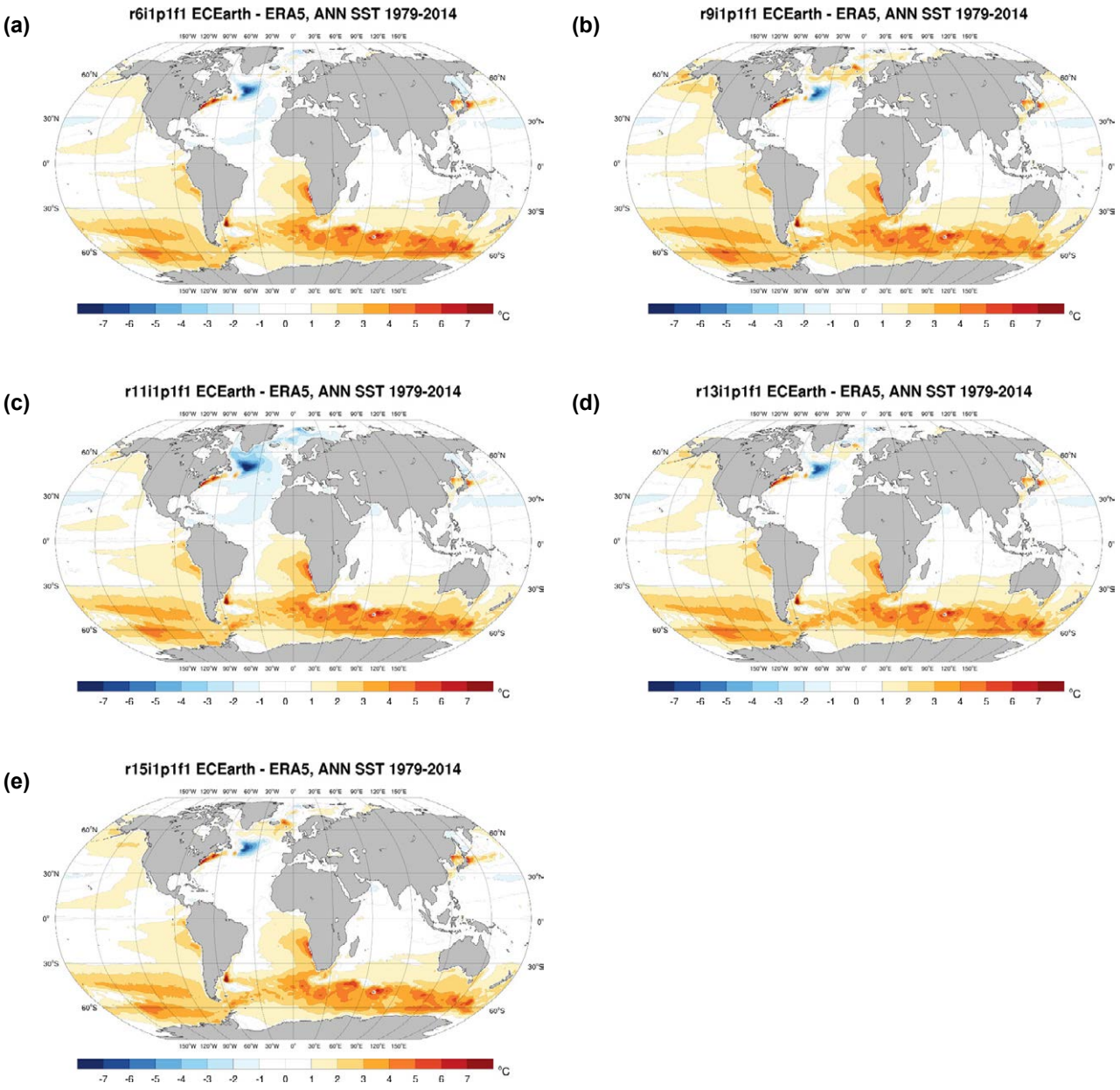

Figure 2.52. EC-Earth annual mean SST bias (°C), 1979–2014 (ERA5 reanalysis minus EC-Earth): (a) EC-Earth r6i1p1f1, (b) EC-Earth r9i1p1f1, (c) EC-Earth r11i1p1f1, (d) EC-Earth r13i1p1f1 and (e) EC-Earth r15i1p1f1.

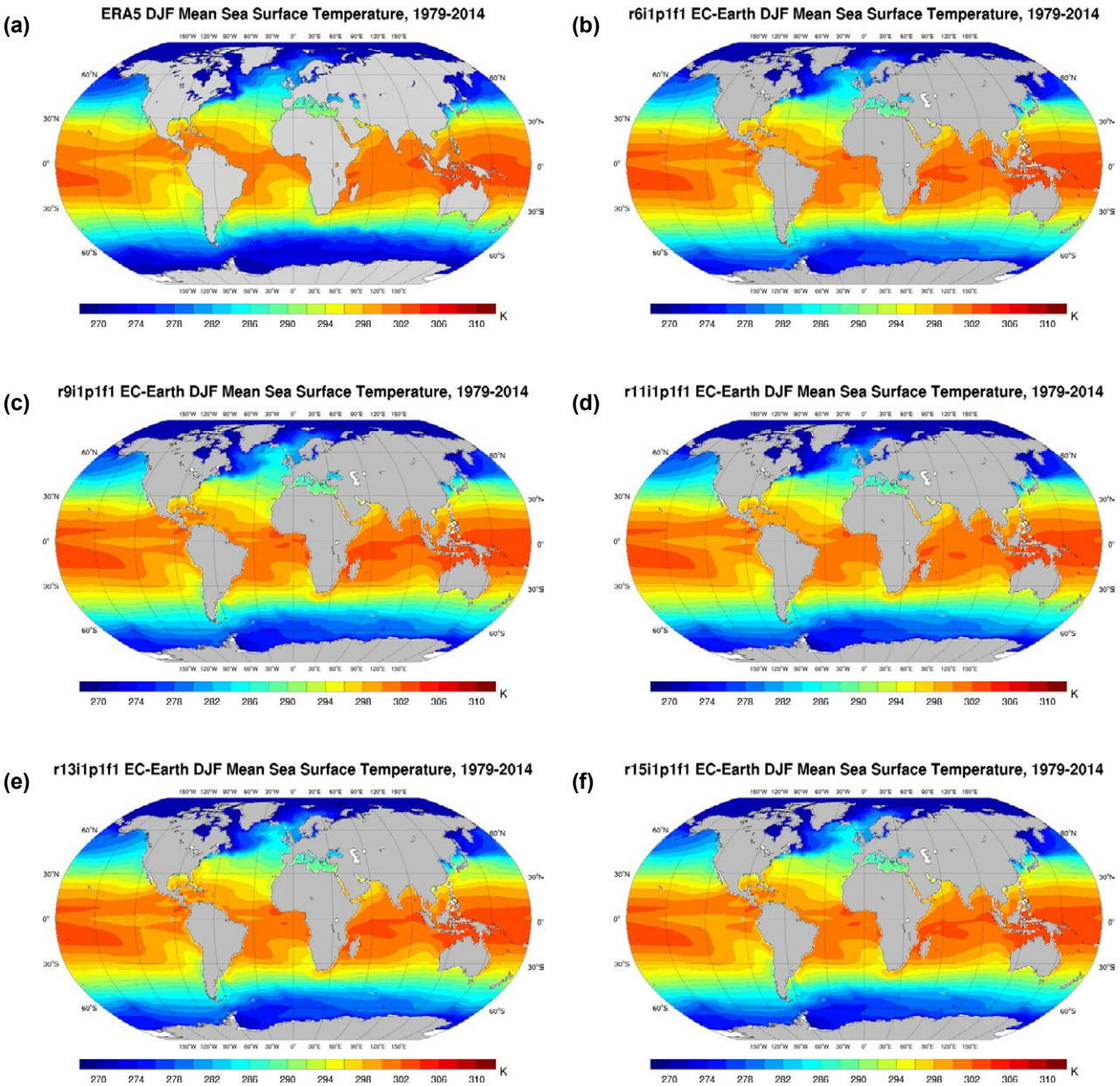

Figure 2.53. Mean SST for DJF (K), 1979–2014: (a) ERA5 reanalysis, (b) EC-Earth r6i1p1f1, (c) EC-Earth r9i1p1f1, (d) EC-Earth r11i1p1f1, (e) EC-Earth r13i1p1f1 and (f) EC-Earth r15i1p1f1.

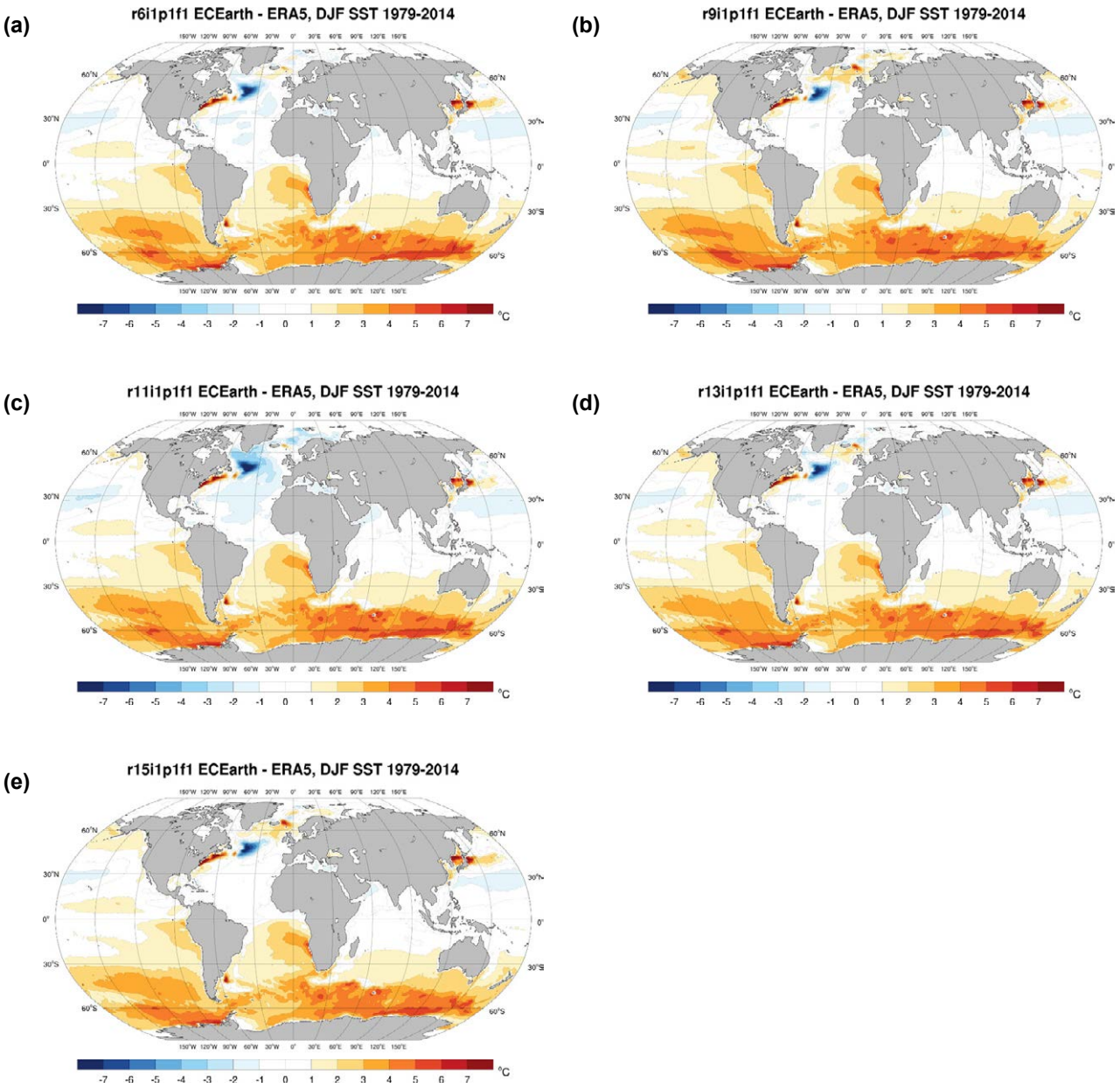

Figure 2.54. EC-Earth mean SST bias (°C) for DJF, 1979–2014 (ERA5 reanalysis minus EC-Earth): (a) EC-Earth r6i1p1f1, (b) EC-Earth r9i1p1f1, (c) EC-Earth r11i1p1f1, (d) EC-Earth r13i1p1f1 and (e) EC-Earth r15i1p1f1.

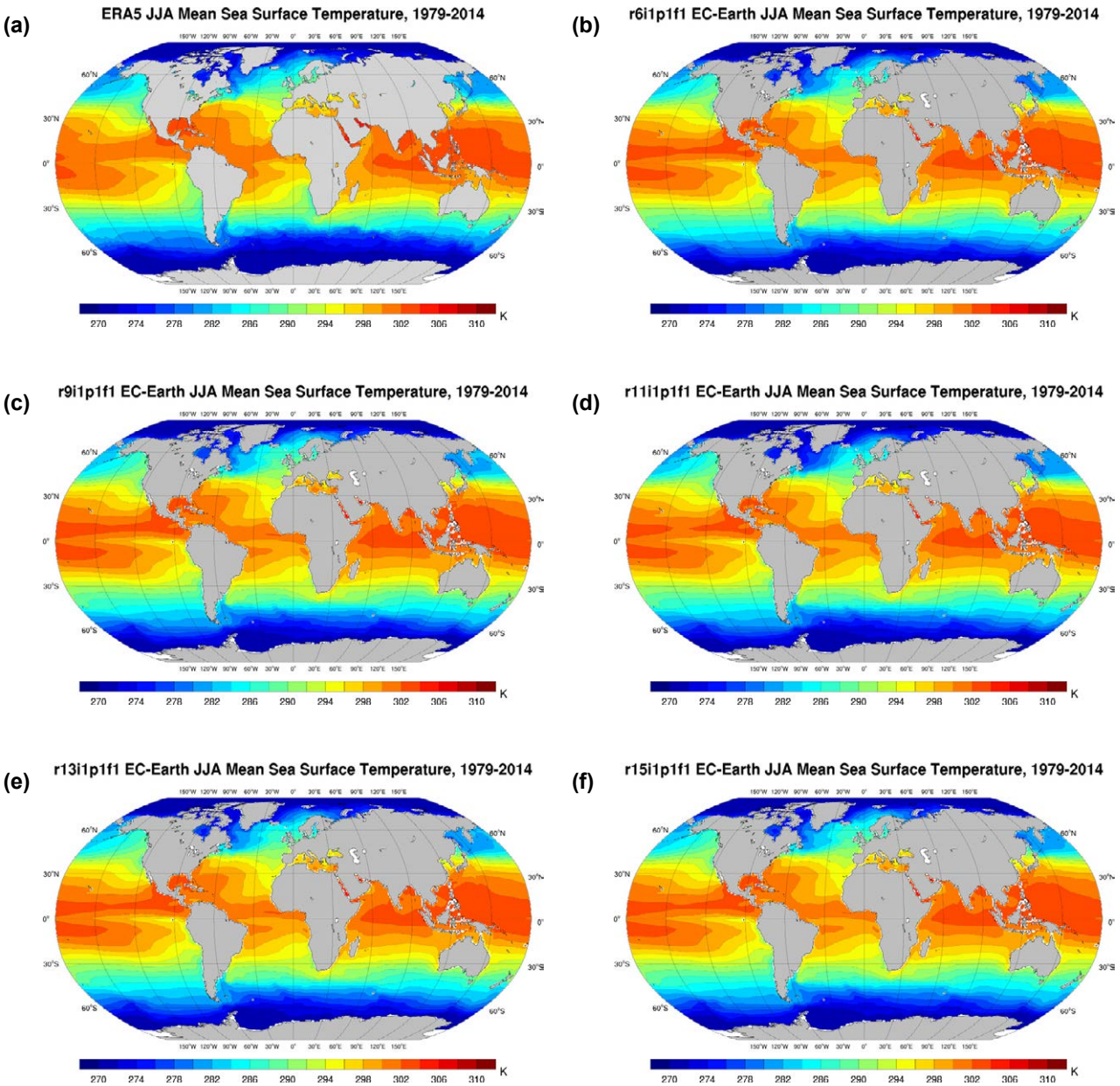

Figure 2.55. Mean SST for JJA (K), 1979–2014: (a) ERA5 reanalysis, (b) EC-Earth r6i1p1f1, (c) EC-Earth r9i1p1f1, (d) EC-Earth r11i1p1f1, (e) EC-Earth r13i1p1f1 and (f) EC-Earth r15i1p1f1.

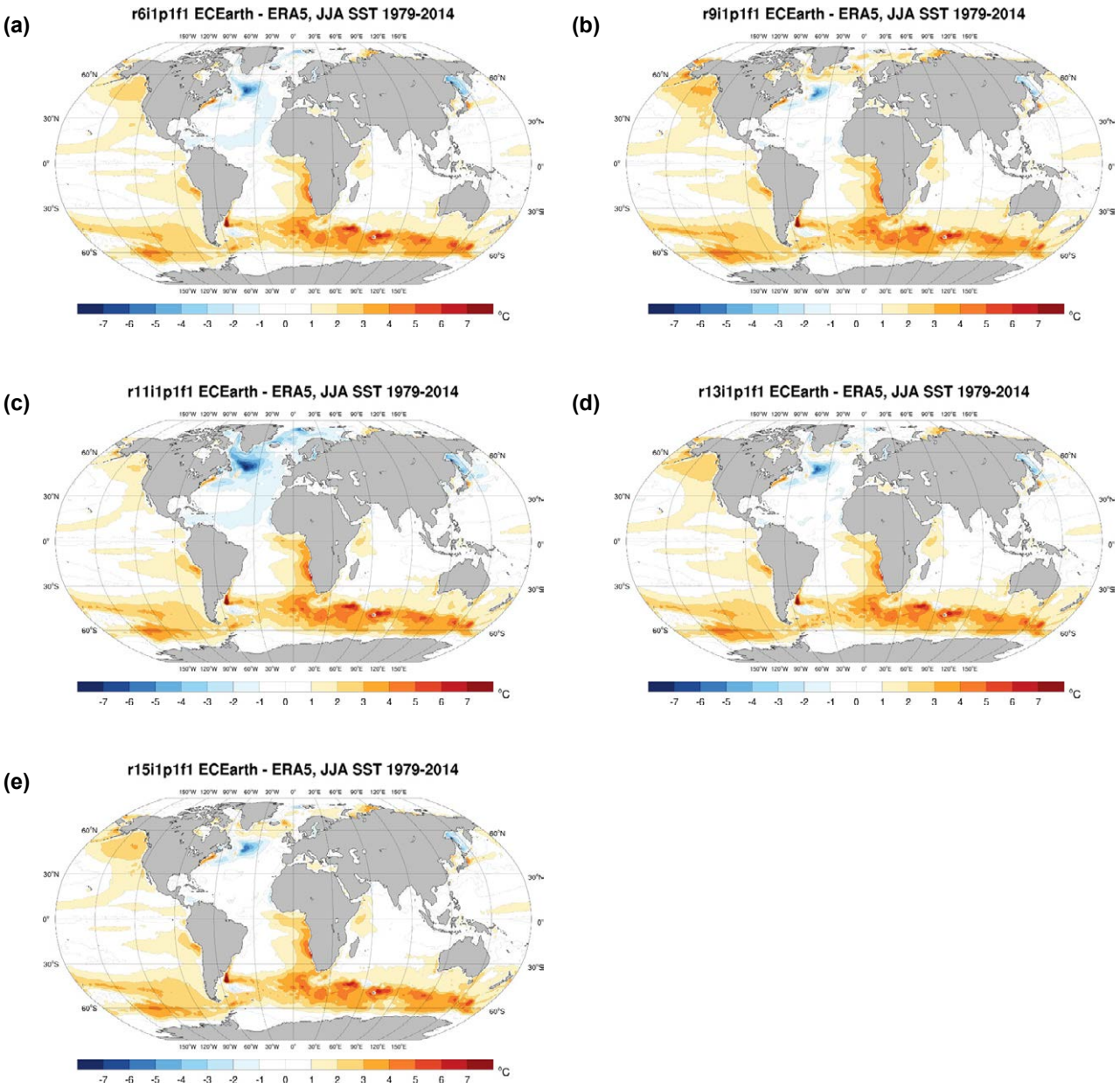

Figure 2.56. EC-Earth mean SST bias (°C) for JJA, 1979–2014 (ERA5 reanalysis minus EC-Earth): (a) EC-Earth r6i1p1f1, (b) EC-Earth r9i1p1f1, (c) EC-Earth r11i1p1f1, (d) EC-Earth r13i1p1f1 and (e) EC-Earth r15i1p1f1.

Table 2.9. Mean and minimum bias (°C) over the North Atlantic area 40–60°N, 25–55°W for each of the five EC-Earth ensemble members[a]

Time period	r6i1p1f1		r9i1p1f1		r11i1p1f1		r13i1p1f1		r15i1p1f1	
	Mean	Min.	Mean	Min.	Mean	Min.	Mean	Min.	Mean	Min.
Annual	–1.54	–7.45	–0.58	–6.83	–2.76	–8.70	–1.20	–6.99	–0.92	–6.83
DJF	–1.69	–8.54	–0.76	–8.23	–2.77	–9.67	–1.31	–8.32	–1.07	–8.18
MAM	–1.87	–9.14	–0.92	–8.15	–3.14	–10.7	–1.51	–8.30	–1.19	–7.84
JJA	–1.61	–6.55	–0.53	–5.66	–3.15	–7.89	–1.32	–6.25	–1.05	–5.99
SON	–0.98	–5.59	–0.12	–5.38	–2.00	–6.53	–0.67	–5.40	–0.38	–5.30

[a]In each case the model data are compared with ERA5 reanalysis data for the period 1979–2014.

Table 2.10. Mean global annual and seasonal SST bias (°C) for each of the five EC-Earth ensemble members[a]

Time period	r6i1p1f1		r9i1p1f1		r11i1p1f1		r13i1p1f1		r15i1p1f1	
	Bias	MAE	Bias	MAE	Bias	MAE	Bias	MAE	Bias	MAE
Annual	0.91	1.22	1.13	1.32	0.84	1.30	1.01	1.26	1.03	1.24
DJF	1.10	1.48	1.32	1.59	1.04	1.54	1.19	1.51	1.20	1.47
MAM	1.02	1.52	1.23	1.62	0.96	1.63	1.13	1.58	1.15	1.54
JJA	0.78	1.09	1.0	1.19	0.68	1.17	0.87	1.13	0.91	1.12
SON	0.75	1.03	0.96	1.13	0.67	1.08	0.85	1.07	0.88	1.06

[a]In each case the model data are compared with ERA5 reanalysis data for the period 1979–2014

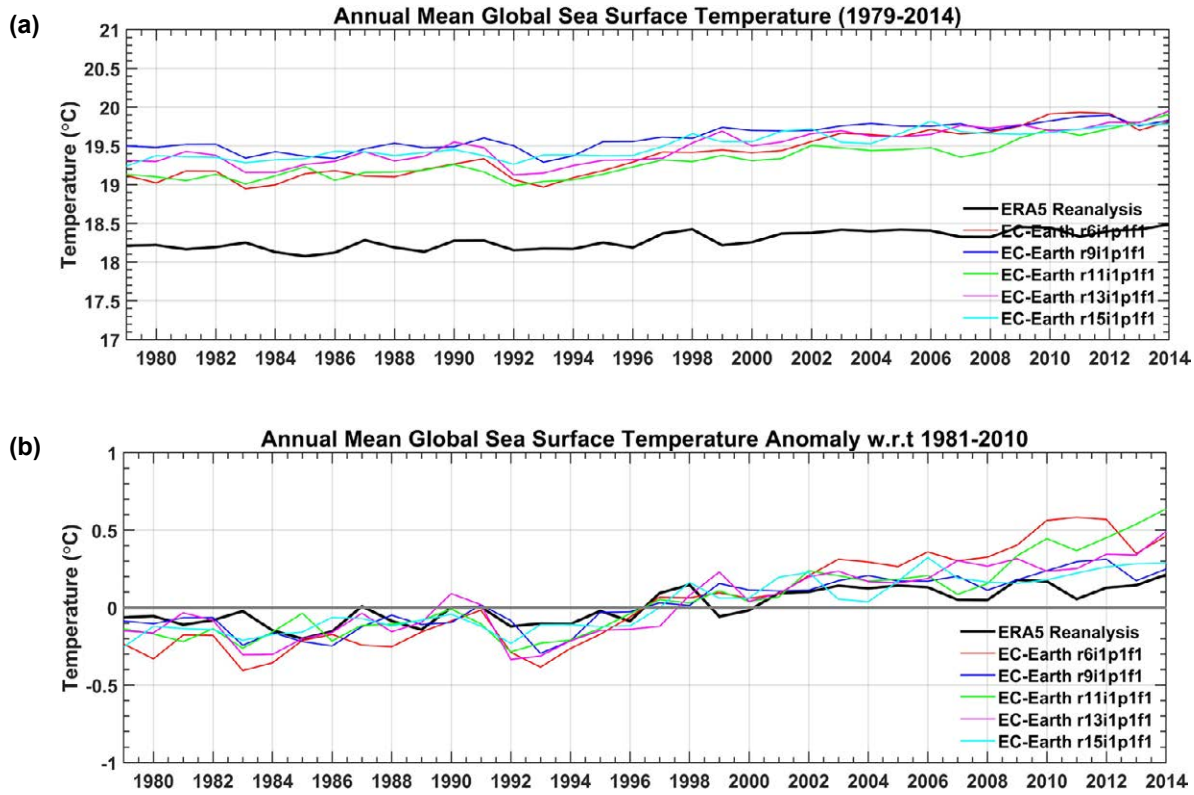

Figure 2.57. Comparison of EC-Earth ensemble members with ERA5 reanalysis data for the period 1979–2014: (a) SST and (b) SST anomalies with respect to the 30-year period 1981–2010.

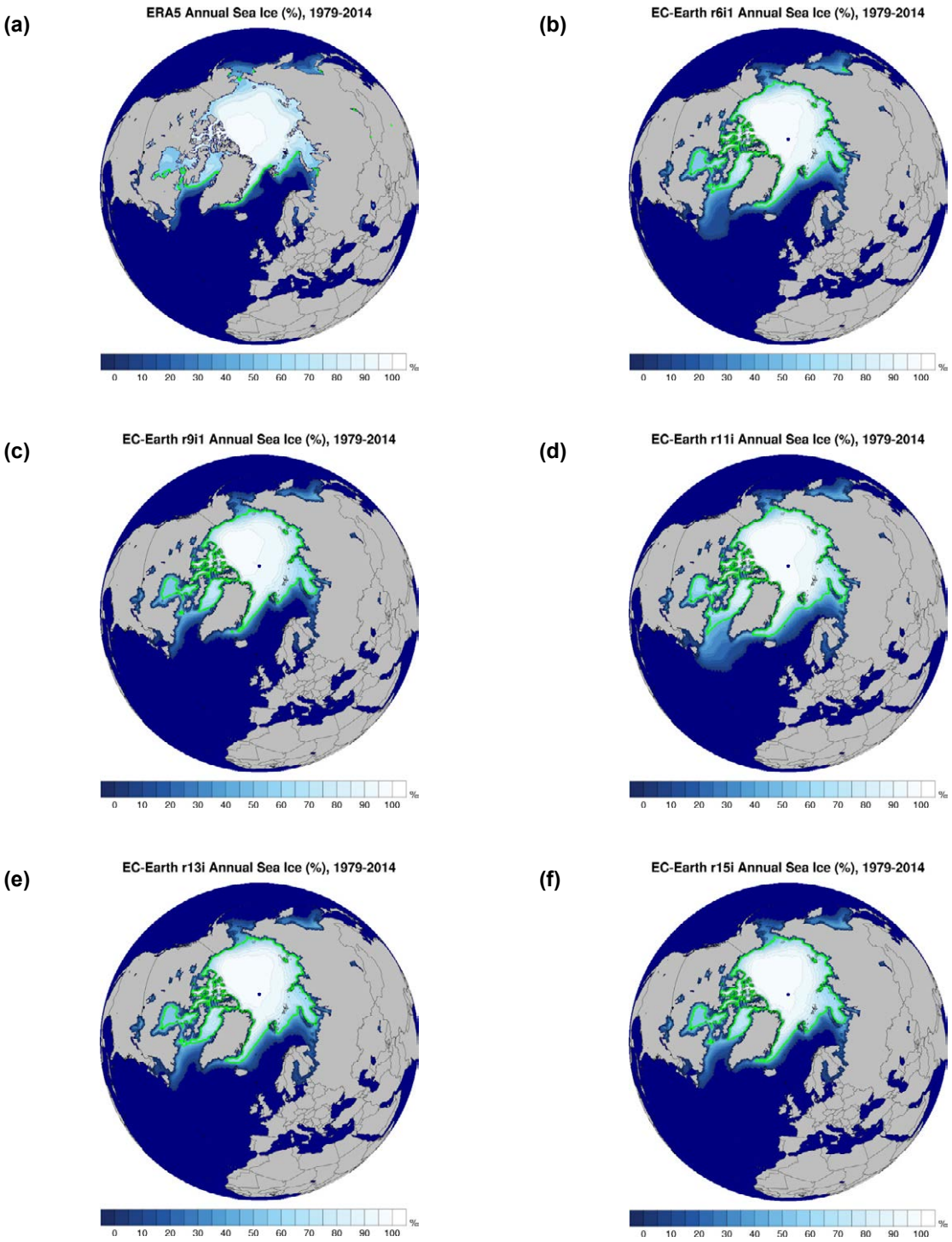

Figure 2.58. Northern Hemisphere annual mean sea ice fraction (%), 1979–2014: (a) ERA5 reanalysis, (b) EC-Earth r6i1p1f1, (c) EC-Earth r9i1p1f1, (d) EC-Earth r11i1p1f1, (e) EC-Earth r13i1p1f1 and (f) EC-Earth r15i1p1f1. The green line shows the 50% contour line.

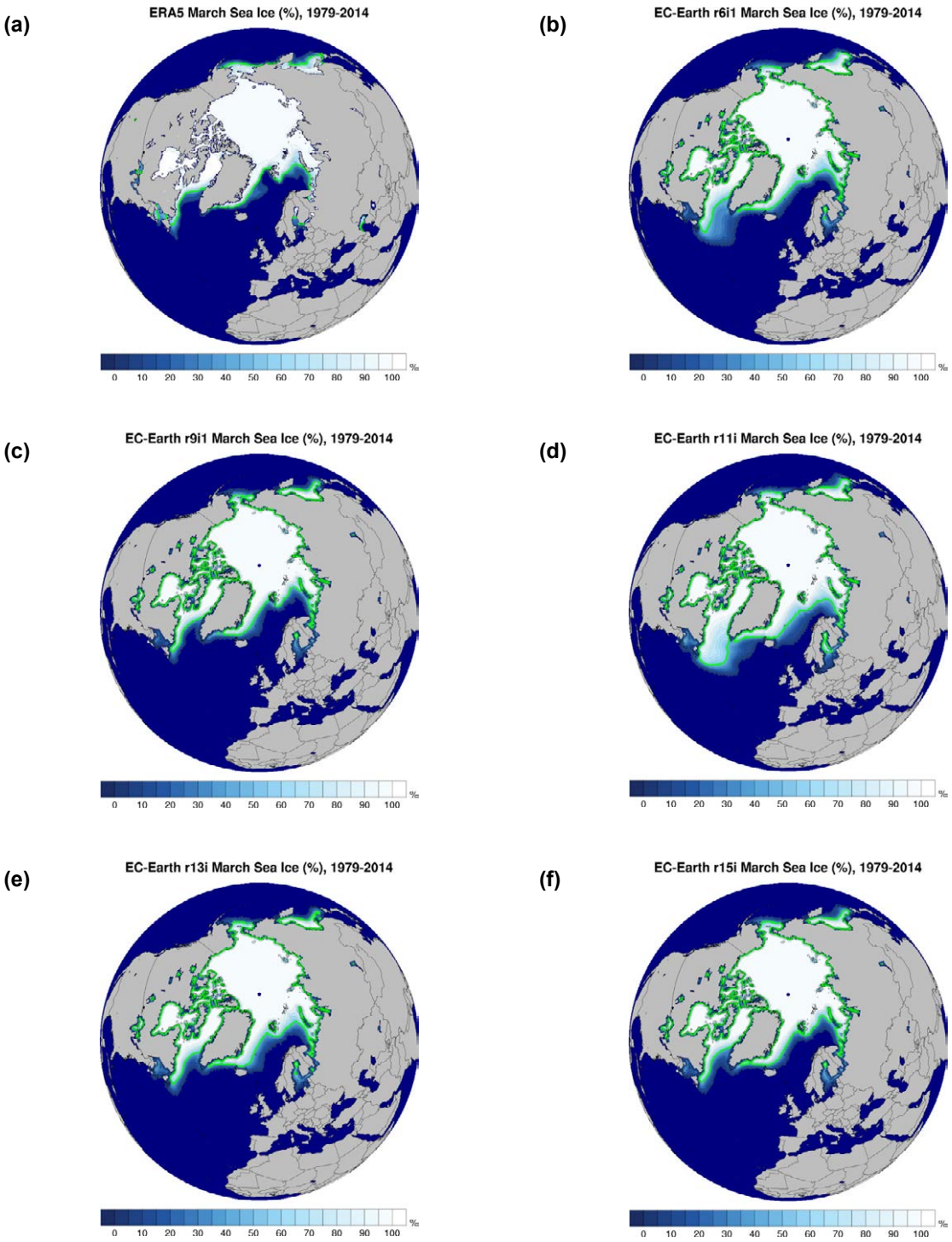

Figure 2.59. Northern Hemisphere March mean sea ice fraction (%), 1979–2014: (a) ERA5 reanalysis, (b) EC-Earth r6i1p1f1, (c) EC-Earth r9i1p1f1, (d) EC-Earth r11i1p1f1, (e) EC-Earth r13i1p1f1 and (f) EC-Earth r15i1p1f1. The green line shows the 50% contour line.

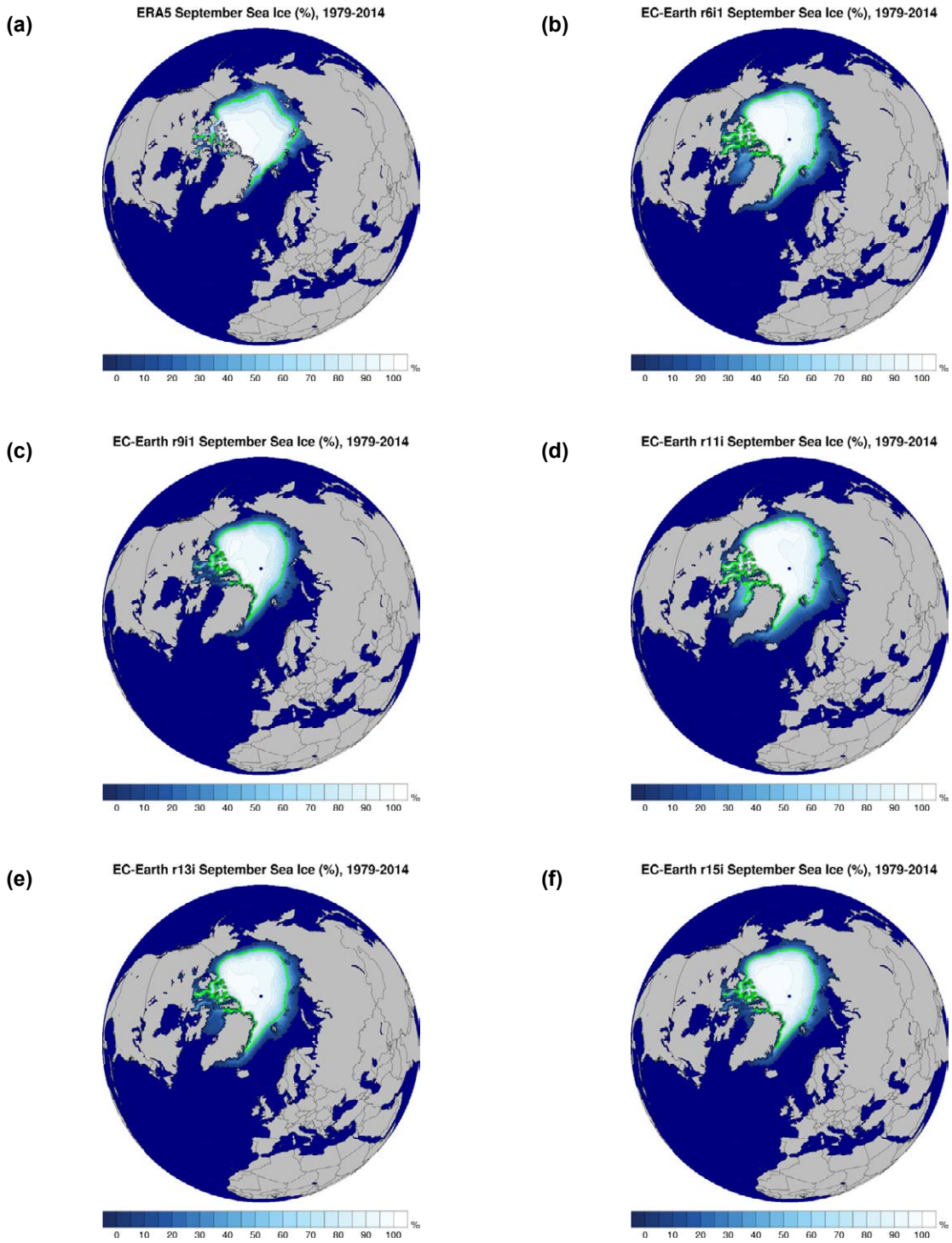

Figure 2.60. Northern Hemisphere September mean sea ice fraction (%), 1979–2014: (a) ERA5 reanalysis, (b) EC-Earth r6i1p1f1, (c) EC-Earth r9i1p1f1, (d) EC-Earth r11i1p1f1, (e) EC-Earth r13i1p1f1 and (f) EC-Earth r15i1p1f1. The green line shows the 50% contour line.

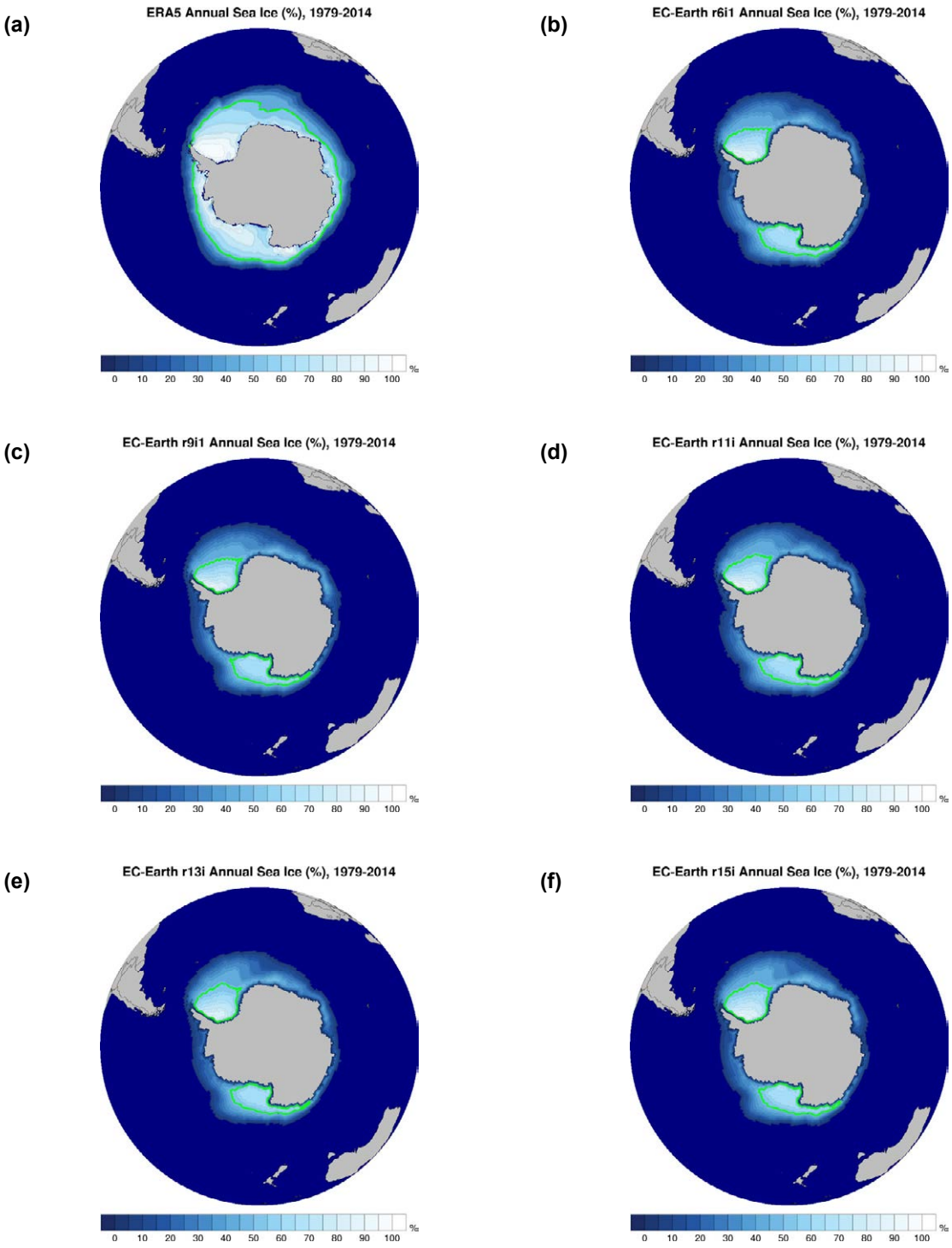

Figure 2.61. Southern Hemisphere annual mean sea ice fraction (%), 1979–2014: (a) ERA5 reanalysis, (b) EC-Earth r6i1p1f1, (c) EC-Earth r9i1p1f1, (d) EC-Earth r11i1p1f1, (e) EC-Earth r13i1p1f1 and (f) EC-Earth r15i1p1f1. The green line shows the 50% contour line.

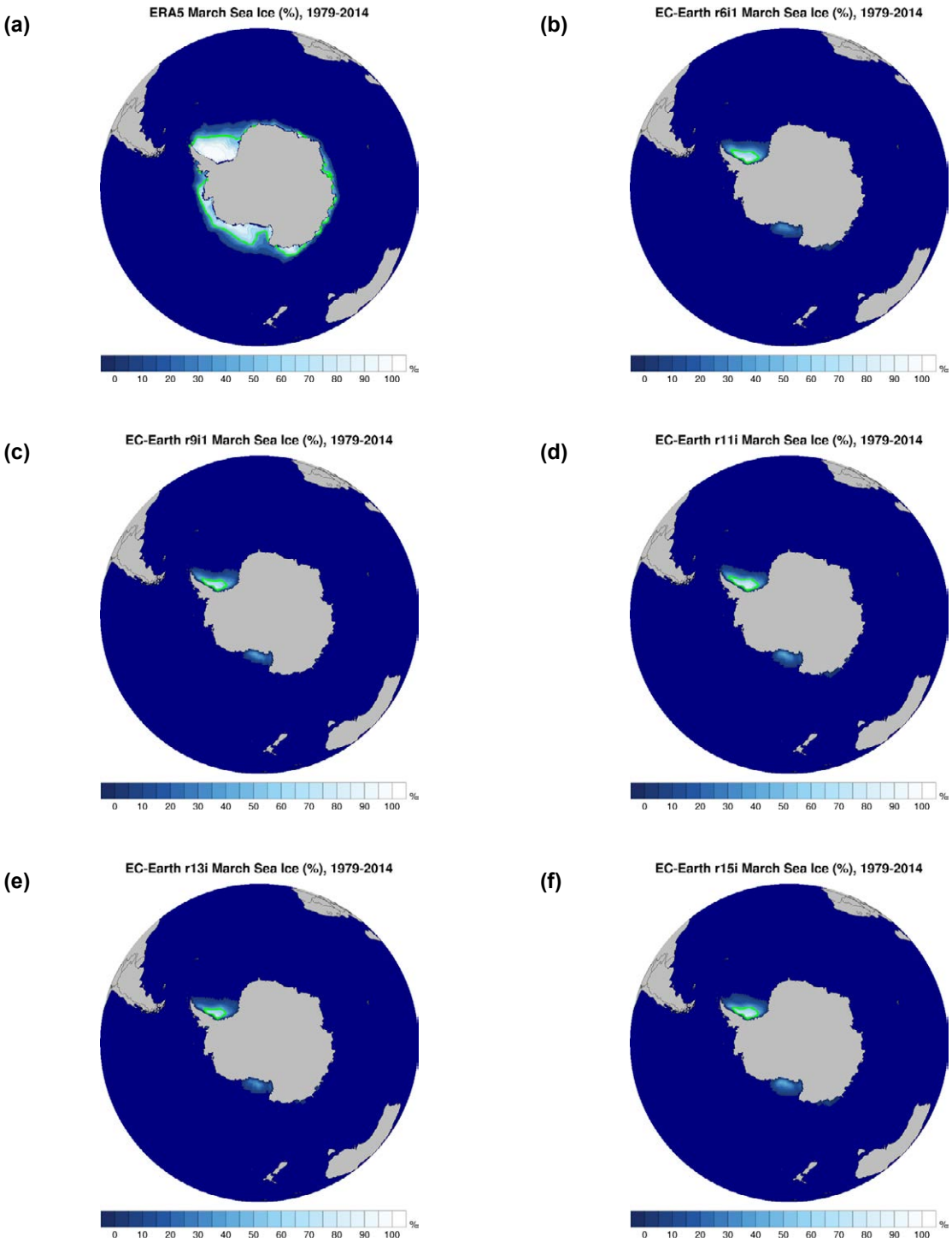

Figure 2.62. Southern Hemisphere March mean sea ice fraction (%), 1979–2014: (a) ERA5 reanalysis, (b) EC-Earth r6i1p1f1, (c) EC-Earth r9i1p1f1, (d) EC-Earth r11i1p1f1, (e) EC-Earth r13i1p1f1 and (f) EC-Earth r15i1p1f1. The green line shows the 50% contour line.

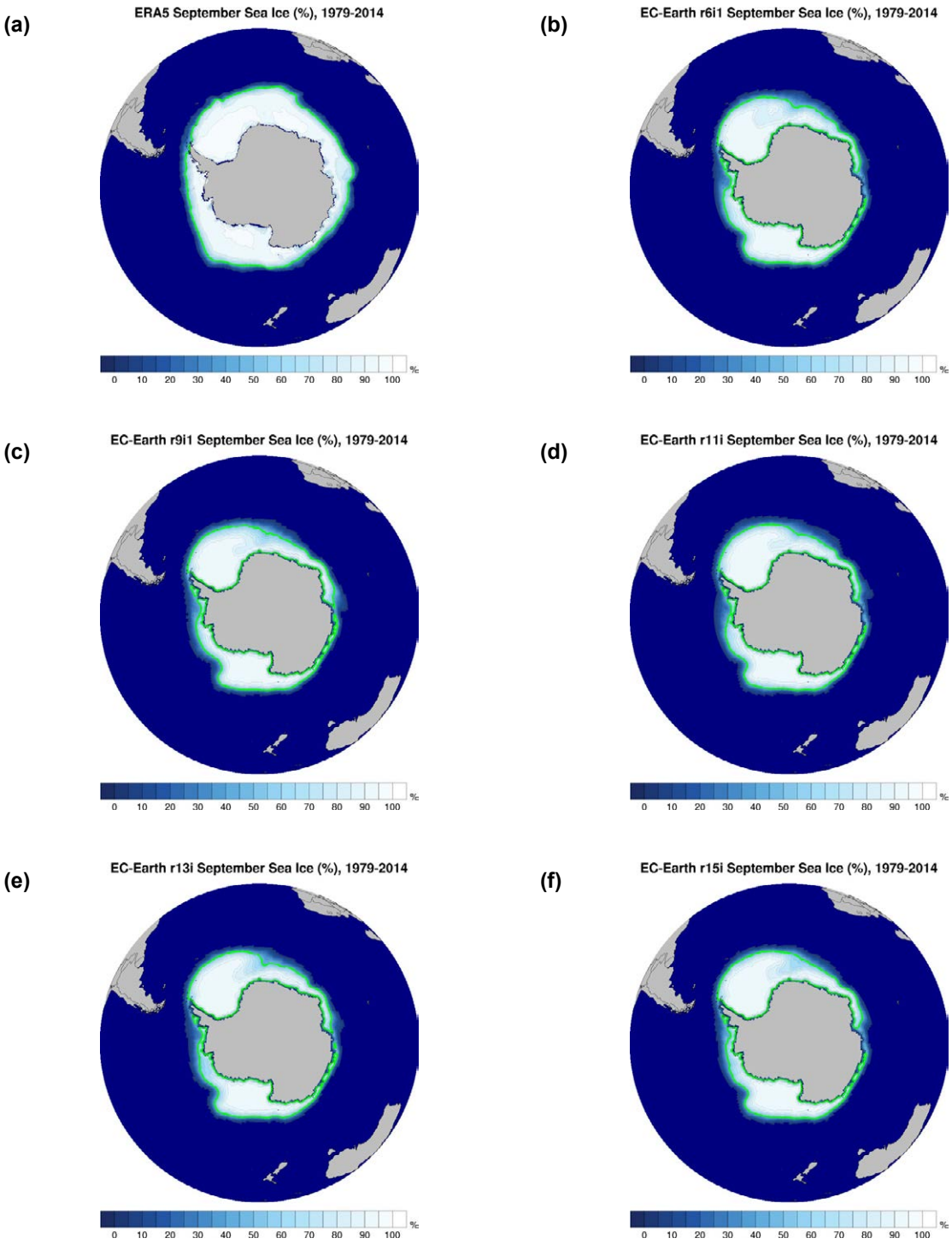

Figure 2.63. Southern Hemisphere September mean sea ice fraction (%), 1979–2014: (a) ERA5 reanalysis, (b) EC-Earth r6i1p1f1, (c) EC-Earth r9i1p1f1, (d) EC-Earth r11i1p1f1, (e) EC-Earth r13i1p1f1 and (f) EC-Earth r15i1p1f1. The green line shows the 50% contour line.

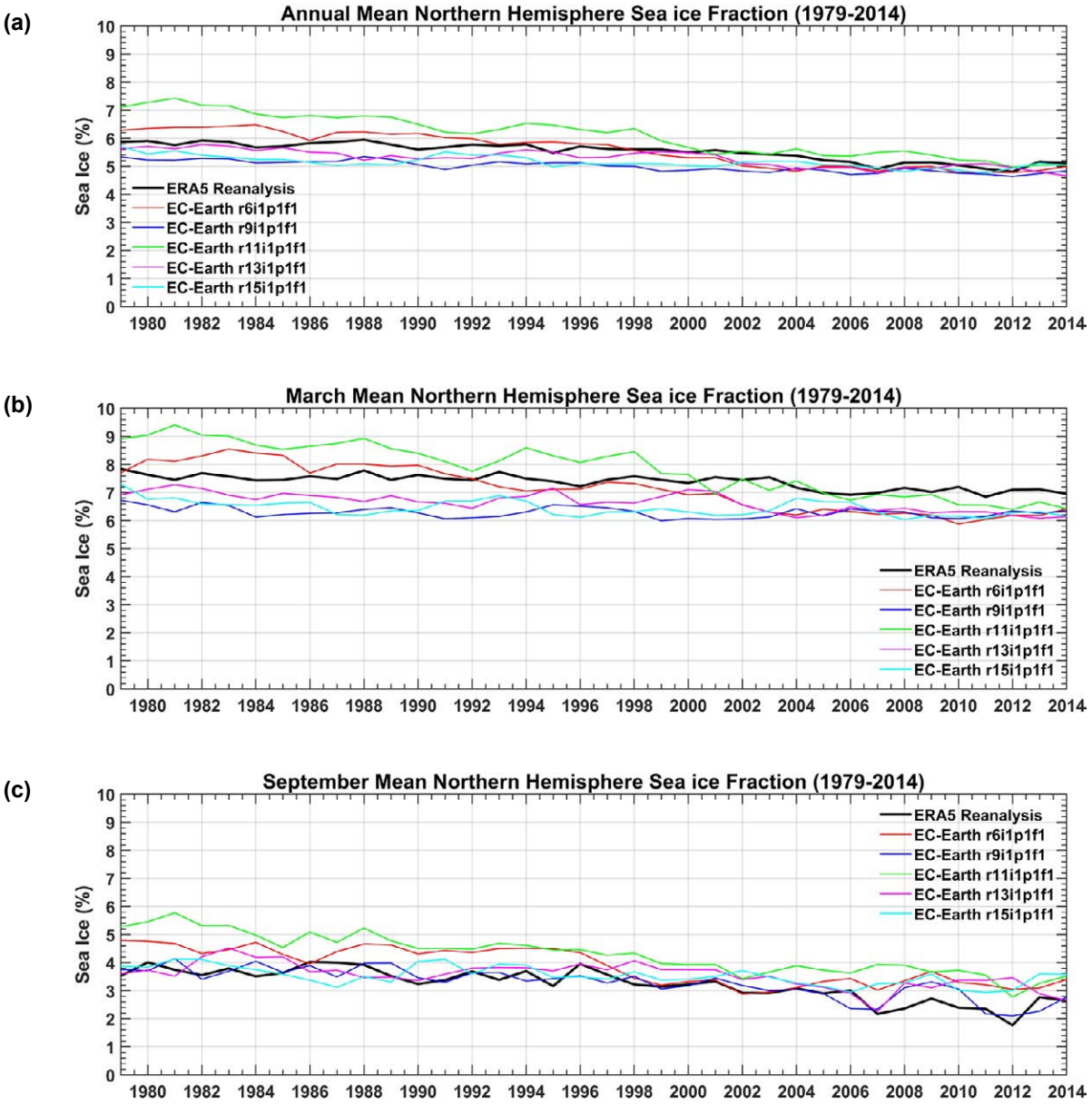

Figure 2.64. Comparison of the EC-Earth Northern Hemisphere sea ice fraction (%) with ERA5 reanalysis data for the period 1979–2014: (a) annual, (b) March and (c) September.

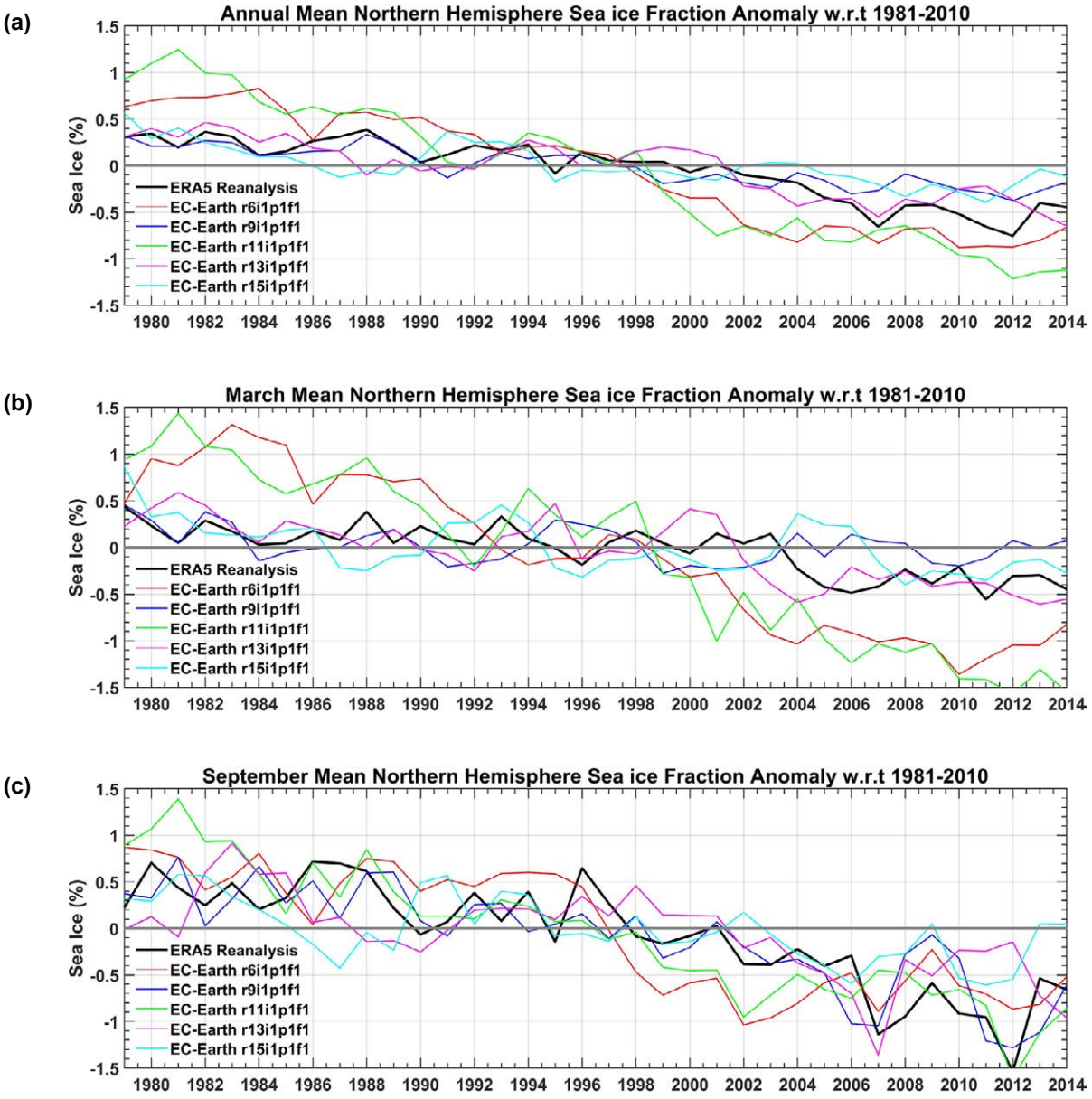

Figure 2.65. Northern Hemisphere sea ice fraction anomalies with respect to the 30-year period 1981–2010: (a) annual, (b) March and (c) September.

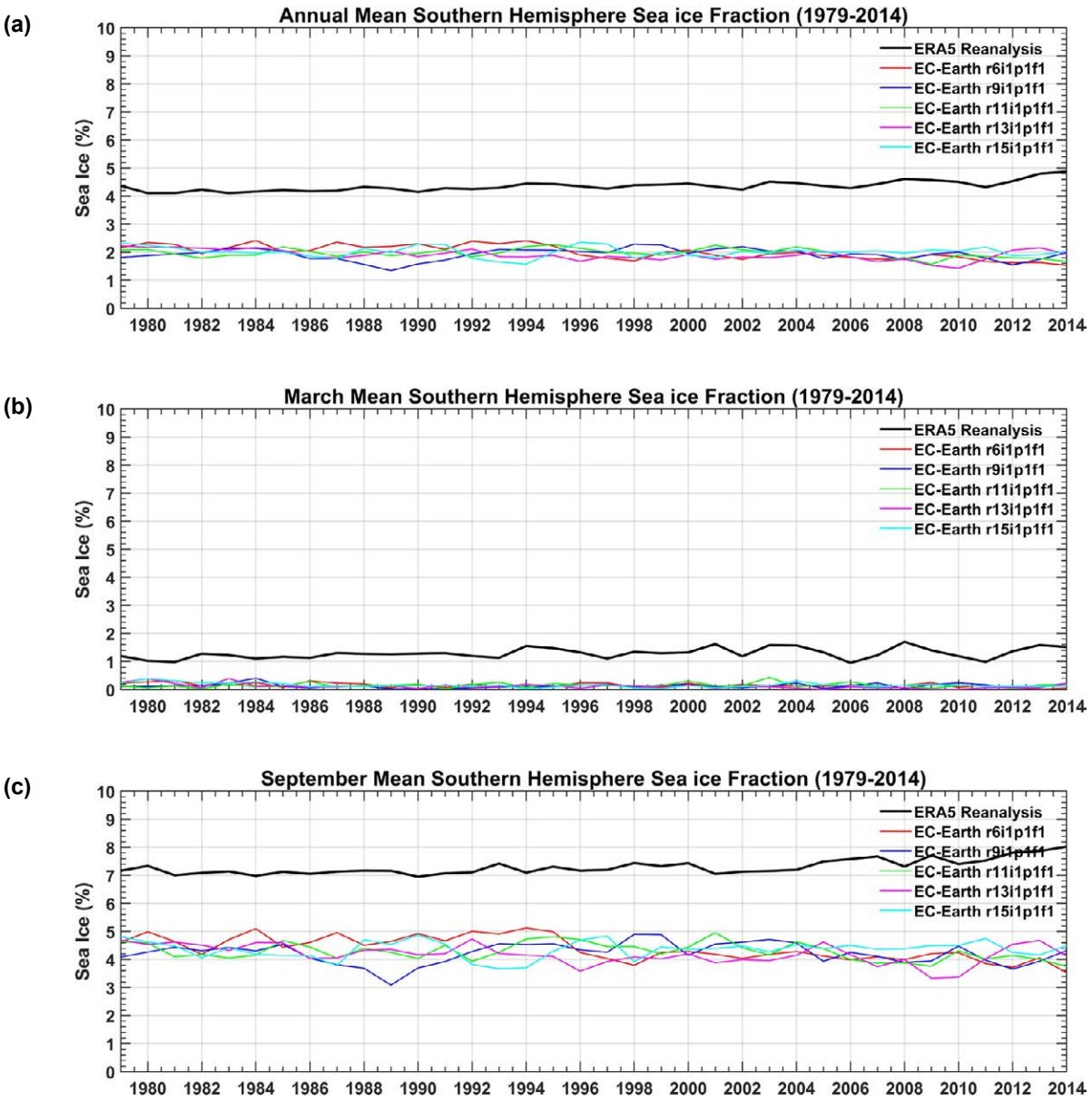

Figure 2.66. Comparison of EC-Earth Southern Hemisphere sea ice fraction (%) with ERA5 reanalysis data for the period 1979–2014: (a) annual, (b) March and (c) September.

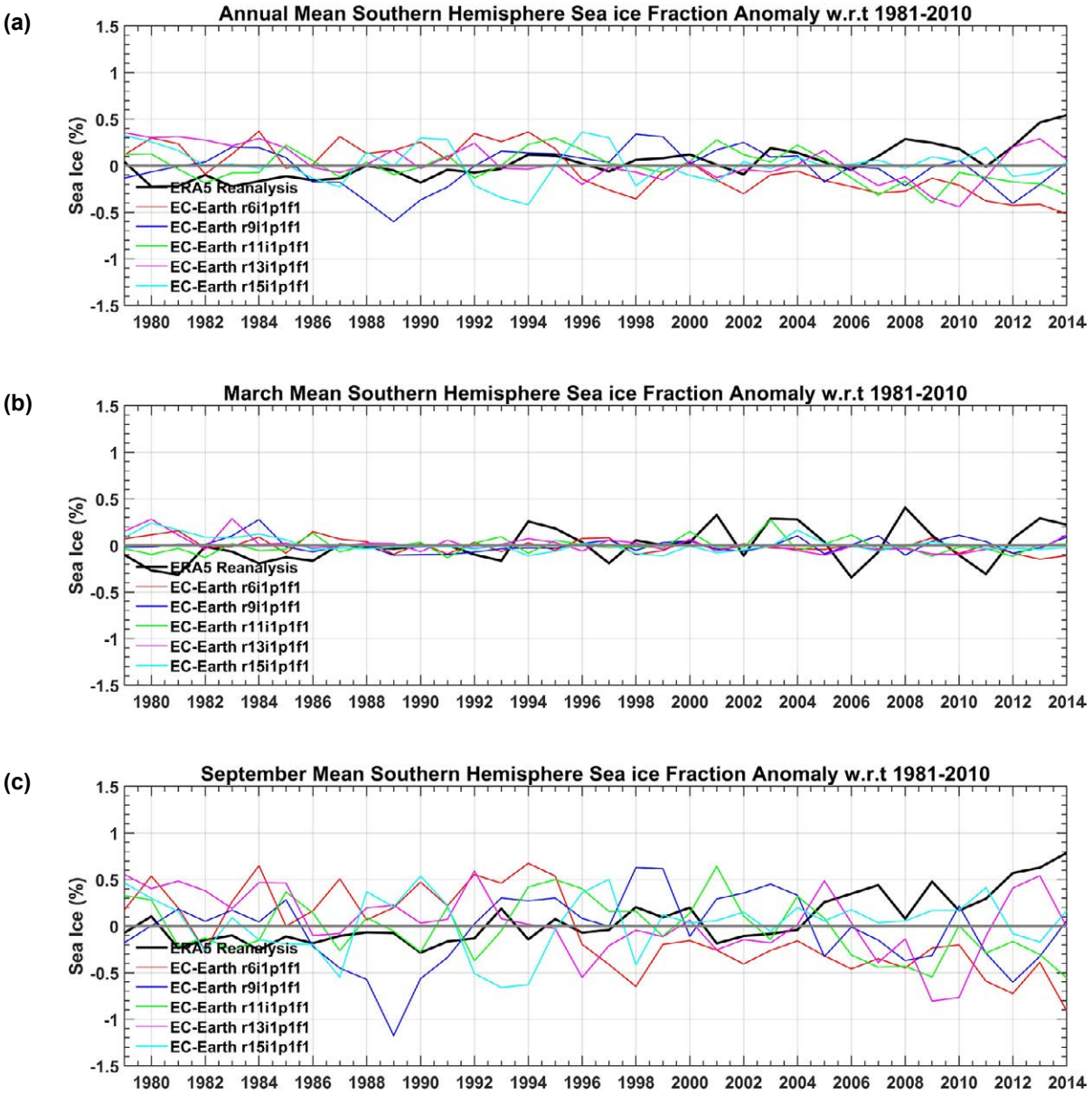

Figure 2.67. Southern Hemisphere sea ice fraction anomalies with respect to the 30-year period 1981–2010: (a) annual, (b) March and (c) September.

3 EC-Earth Climate Projections

The future global climate was simulated by extending each of the five historical (1850–2014) EC-Earth T255-ORCA1L75 experiments to the year 2100 under each of the four ScenarioMIP "tier 1" SSPs. This results in 20 future global climate experiments (five ensembles multiplied by four scenarios). Table 3.1 provides an overview of these simulations.

Projections of climate change were assessed by comparing the two 30-year future periods 2041–2070 and 2071–2100 with the 30-year historical period 1981–2010. Climate projections are presented for the Northern Hemisphere winter (DJF), the Northern Hemisphere summer (JJA) and over the full year. For the climate projections presented here, the mean of the five ensemble members for each SSP was analysed. For example, Figure 3.1a presents the mean of the five SSP1–2.6 ensemble projections for the period 2041–2070.

To quantify the spread (or disagreement) between ensemble members, the standard deviation of the ensemble of climate projections was analysed. For example, Figure 3.8a (the standard deviation of the five SSP1–2.6 ensemble projections of 2-m temperature for the period 2071–2100) demonstrates a small spread (high agreement) between ensemble members except for the regions south of Greenland and the Arctic, north of Scandinavia. This analysis provides a measure of climate projection uncertainty and highlights areas where the ensemble members agree/disagree.[4] It was found that the spread remains consistent between seasons and so the standard deviation statistical figures are limited to the annual projections. Furthermore, only the period 2071–2100 was analysed as it was found that the corresponding statistics for 2041–2070 typically showed similar but smaller values.

3.1 2-m Temperature Projections

Figure 3.1 presents the spatial distribution of annual mean 2-m temperature projections for each of the four SSPs for the 30-year period 2041–2070 (relative to 1981–2010). The corresponding 2071–2100 projections are presented in Figure 3.2. Note that for each figure, the mean of the five ensemble members is considered. The largest increases in temperatures are seen over the land masses, in particular the northern-most regions and the Arctic. Projections of temperature increase range from ~0.5°C over the Southern Hemisphere oceans for 2041–2070 SSP1–2.6 (Figure 3.1a) to ~18°C over the Arctic for 2071–2100 SSP5–8.5 (Figure 3.2d).

Projections for DJF (Figures 3.3 and 3.4) follow a similar trend except that increases in temperature over the northern land masses and the Arctic are enhanced. The projections for JJA (Figures 3.5 and 3.6) follow a similar trend to the annual projections except that increases in temperature over the northern land mases and the Arctic are diminished whereas increases in temperature over Antarctica are enhanced.

Table 3.1. Overview of the Scenario-MIP simulations

EC-Earth ensemble member	SSPs	Model levels archived
r6i1p1f1	SSP1–2.6, SSP2–4.5, SSP3–7.0 and SSP5–8.5	No
r9i1p1f1	SSP1–2.6, SSP2–4.5, SSP3–7.0 and SSP5–8.5	No
r11i1p1f1	SSP1–2.6, SSP2–4.5, SSP3–7.0 and SSP5–8.5	Yes
r13i1p1f1	SSP1–2.6, SSP2–4.5, SSP3–7.0 and SSP5–8.5	No
r15i1p1f1	SSP1–2.6, SSP2–4.5, SSP3–7.0 and SSP5–8.5	No

4 To obtain a robust quantification of the uncertainty of the EC-Earth climate projections, a large ensemble is required. Future work will extend this analysis to include the full ensemble of EC-Earth CMIP6 simulations produced by the consortium.

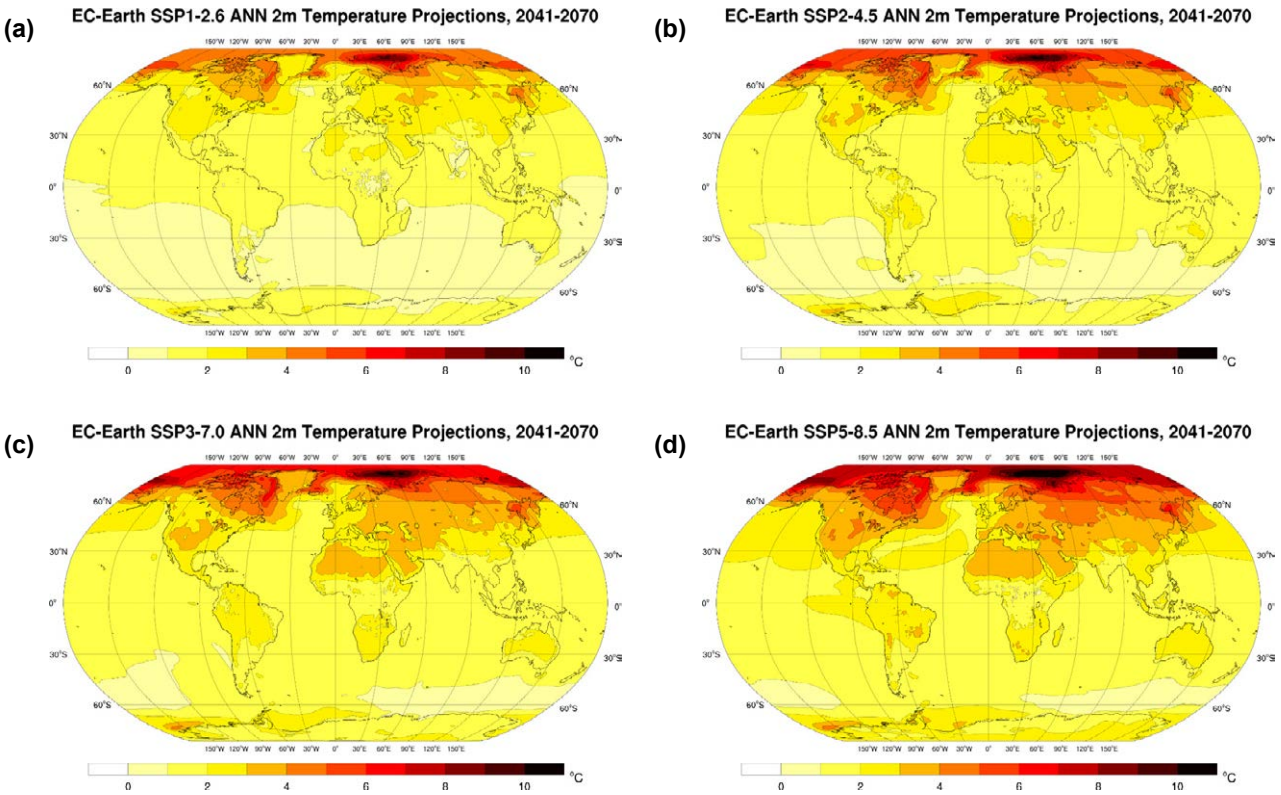

Figure 3.1. EC-Earth annual 2-m temperature projections (2041–2070 vs 1981–2010,°C change): (a) SSP1–2.6, (b) SSP2–4.5, (c) SSP3–7.0 and (d) SSP5–8.5. In each case, an average is taken of the ensemble members r6i1p1f1, r9i1p1f1, r11i1p1f1, r13i1p1f1 and r15i1p1f1.

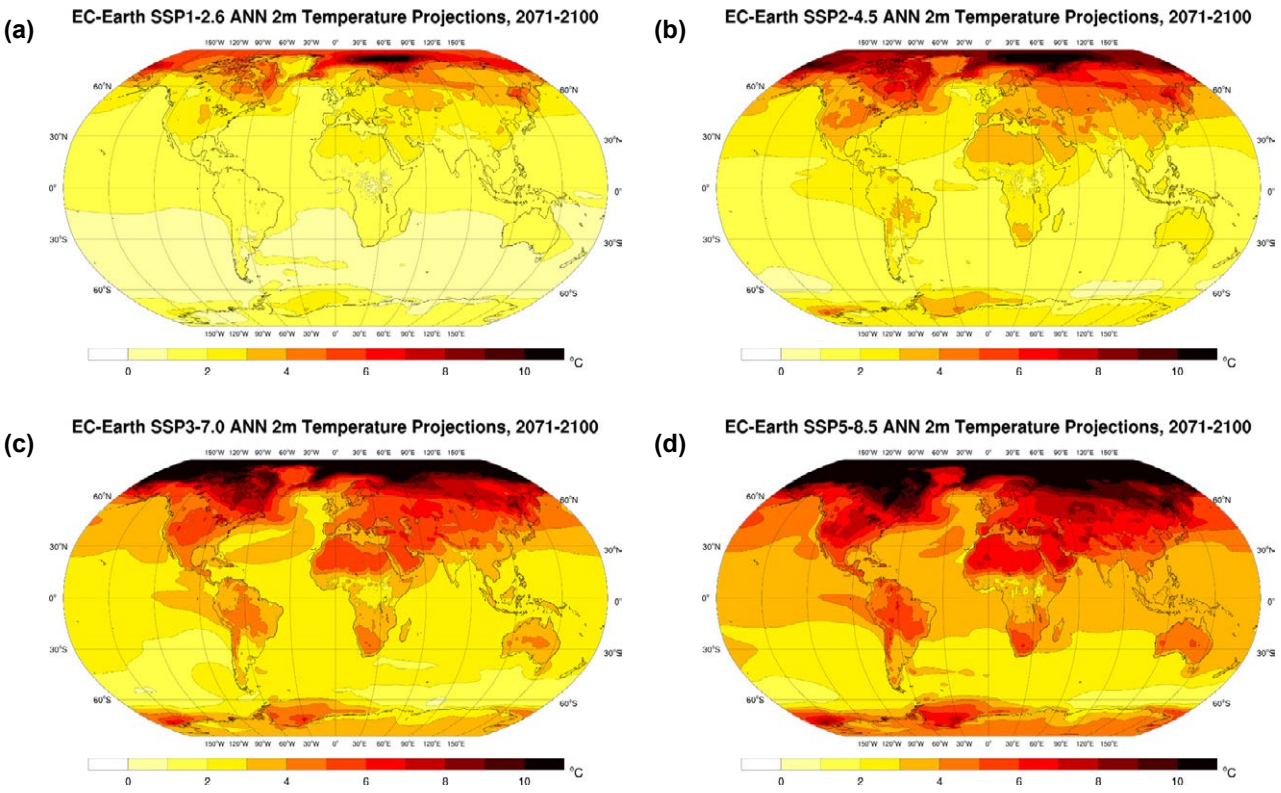

Figure 3.2. EC-Earth annual 2-m temperature projections (2071–2100 vs 1981–2010,°C change): (a) SSP1–2.6, (b) SSP2–4.5, (c) SSP3–7.0 and (d) SSP5–8.5. In each case, an average is taken of the ensemble members r6i1p1f1, r9i1p1f1, r11i1p1f1, r13i1p1f1 and r15i1p1f1.

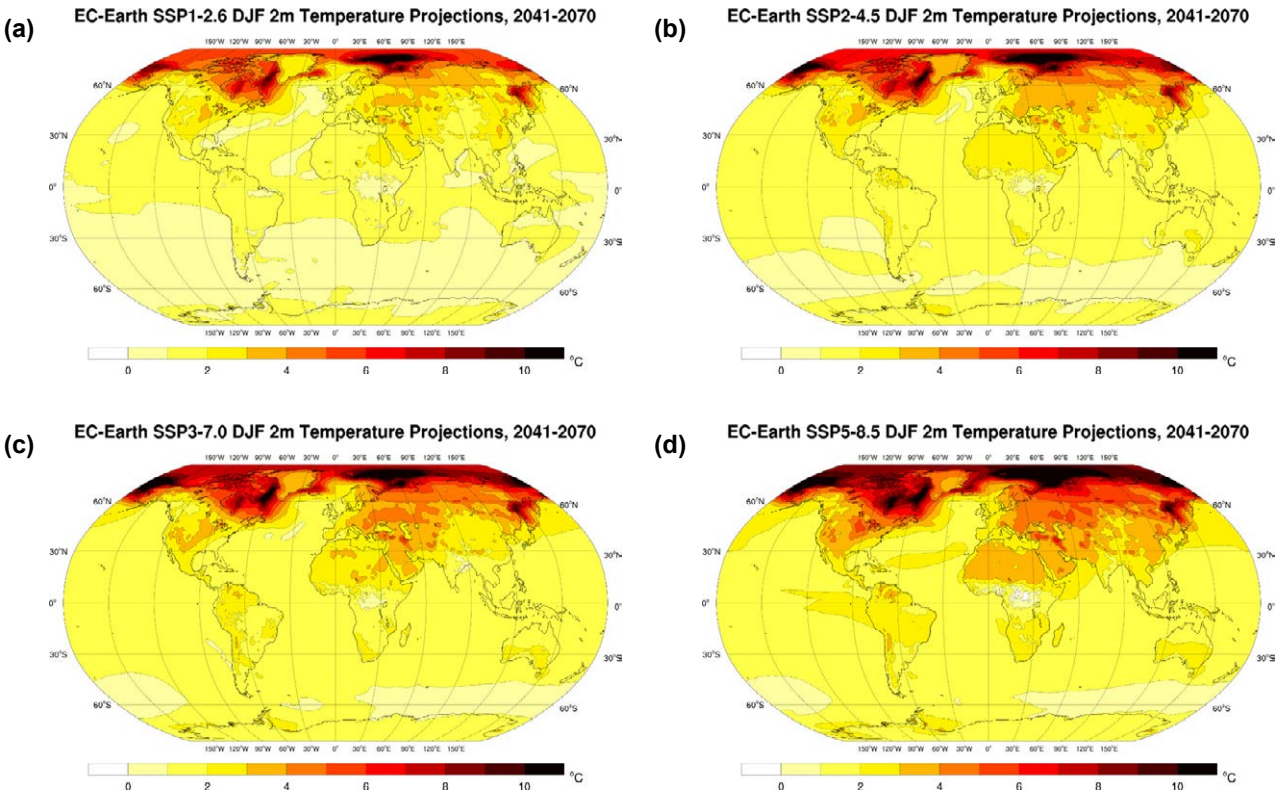

Figure 3.3. EC-Earth DJF 2-m temperature projections (2041–2070 vs 1981–2010,°C change): (a) SSP1–2.6, (b) SSP2–4.5, (c) SSP3–7.0 and (d) SSP5–8.5. In each case, an average is taken of the ensemble members r6i1p1f1, r9i1p1f1, r11i1p1f1, r13i1p1f1 and r15i1p1f1.

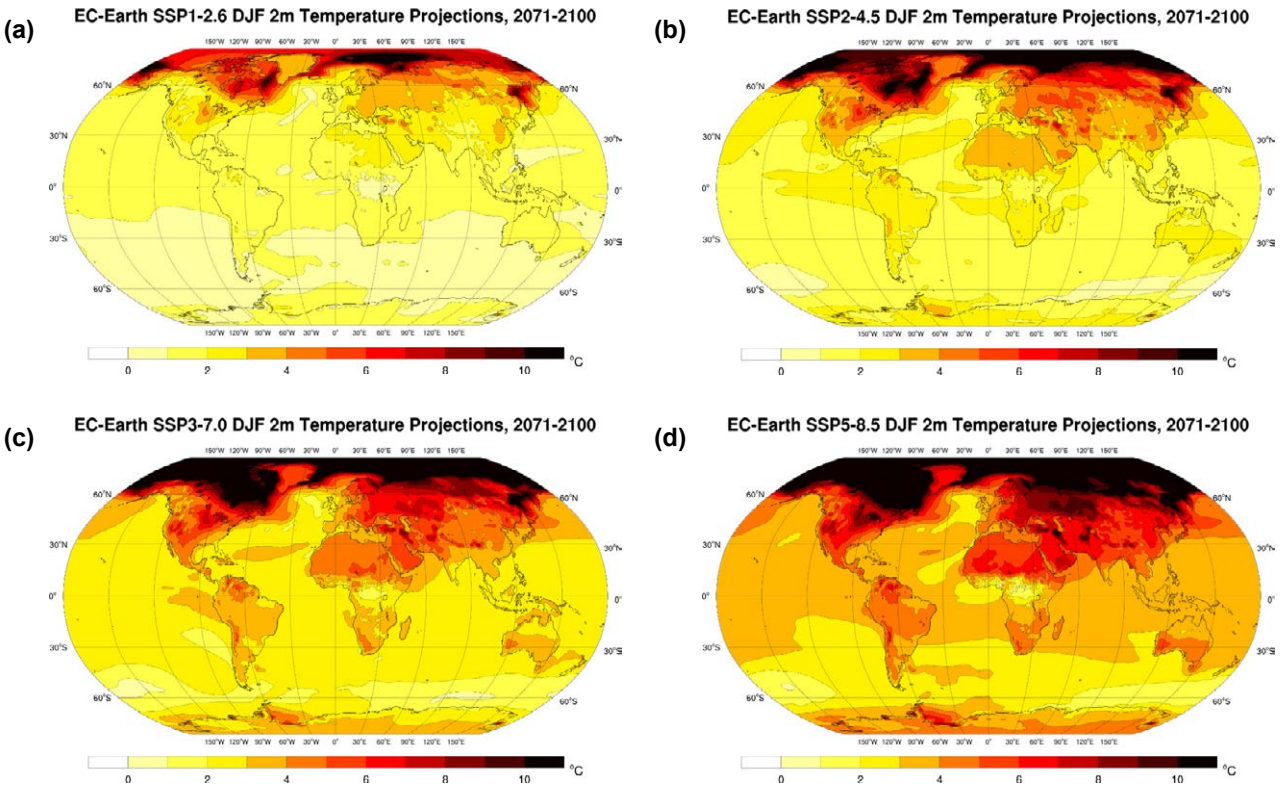

Figure 3.4. EC-Earth DJF 2-m temperature projections (2071–2100 vs 1981–2010,°C change): (a) SSP1–2.6, (b) SSP2–4.5, (c) SSP3–7.0 and (d) SSP5–8.5. In each case, an average is taken of the ensemble members r6i1p1f1, r9i1p1f1, r11i1p1f1, r13i1p1f1 and r15i1p1f1.

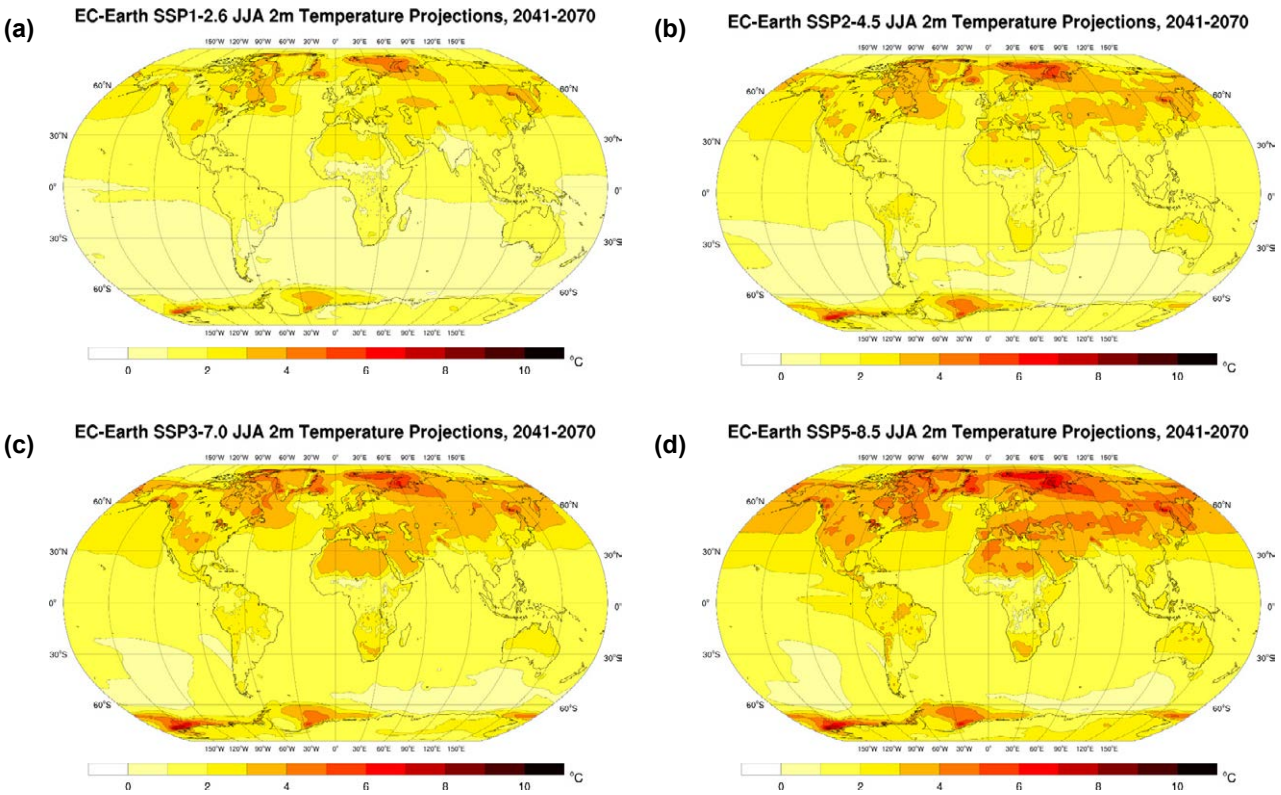

Figure 3.5. EC-Earth JJA 2-m temperature projections (2041–2070 vs 1981–2010,°C change): (a) SSP1–2.6, (b) SSP2–4.5, (c) SSP3–7.0 and (d) SSP5–8.5. In each case, an average is taken of the ensemble members r6i1p1f1, r9i1p1f1, r11i1p1f1, r13i1p1f1 and r15i1p1f1.

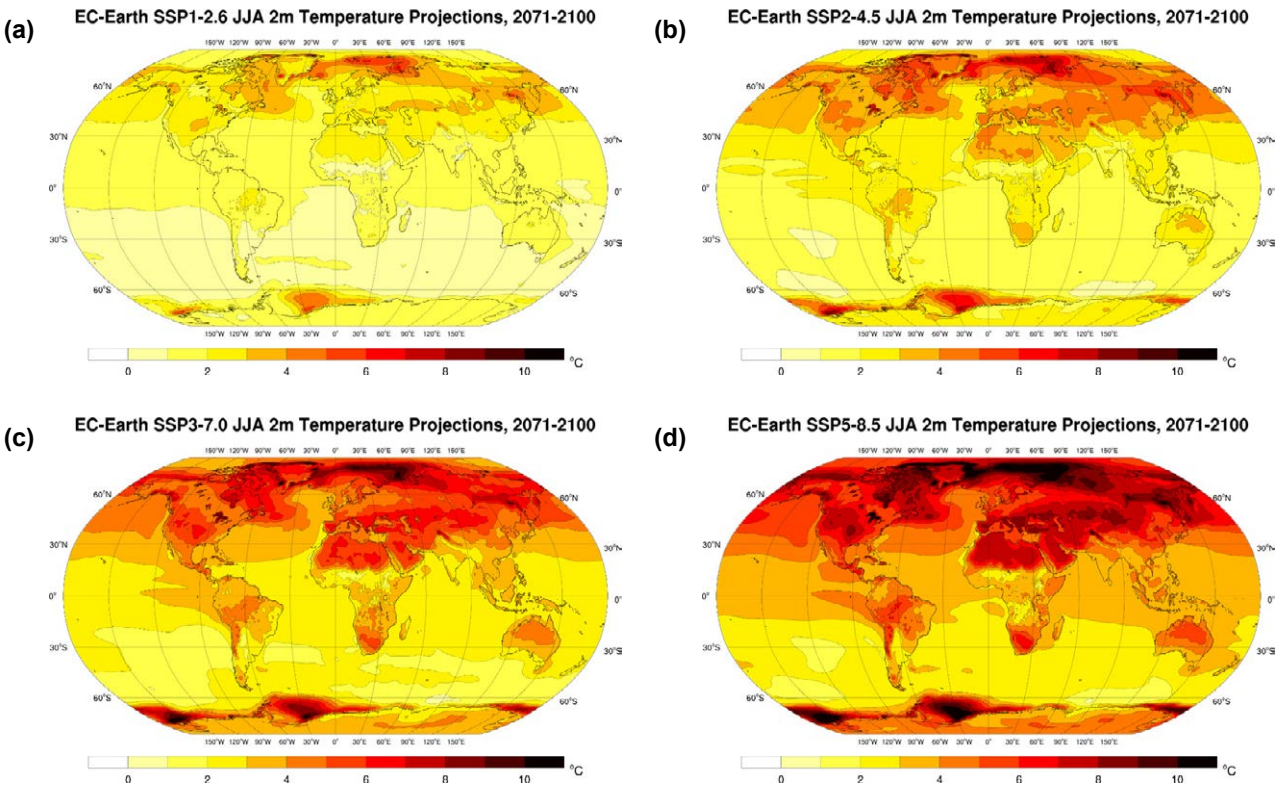

Figure 3.6. EC-Earth JJA 2-m temperature projections (2071–2100 vs 1981–2010,°C change): (a) SSP1–2.6, (b) SSP2–4.5, (c) SSP3–7.0 and (d) SSP5–8.5. In each case, an average is taken of the ensemble members r6i1p1f1, r9i1p1f1, r11i1p1f1, r13i1p1f1 and r15i1p1f1.

Note that the large projected increases in the Arctic region should be viewed in the context of the low mean temperatures in this region. The mean annual 2-m temperature in the Arctic Circle (latitudes above 66.5°), derived from ERA5 1979–2014 data, is –10.9°C, with values ranging from –28.2°C over Greenland to 6.7°C over the Greenland Sea. Similarly, the mean DJF and JJA 2-m temperatures in the Arctic Circle are –22.9°C (ranging from –40.9°C to 3.7°C) and 2.7°C (ranging from –15.2°C to 16.5°C), respectively.

The mean global annual temperature anomalies (relative to 1981–2010) for all five historical simulations (1850–2014) and 20 SSPs (2015–2100) are presented in Figure 3.7. The bold lines represent the ensemble means. All ensemble members show a steady increase in temperature from around 2000, with a noticeable divergence between the SSPs from around 2050. By the year 2100, the global mean temperature is projected to increase by approximately 1.5°C, 2.8°C, 4.2°C and 5.5°C for SSP1–2.6, SSP2–4.5, SSP3–7.0 and SSP5–8.5, respectively. The small spread between the individual ensemble members demonstrates a high level of agreement. This is confirmed by Figure 3.8, which shows the standard deviation of each SSP ensemble of climate projections. High levels of agreement between ensembles are noted for all regions except south of Greenland and the Arctic region north of Scandinavia. A closer analysis of the individual ensemble members shows that the disagreement in the northern regions is the result of a difference between two groups – the r6i1p1f1 and r11i1p1f1 ensemble members project higher (lower) temperature rises than the r9i1p1f1, r13i1p1f1 and r15i1p1f1 ensemble members in the regions roughly north (south) of Iceland. Assigning attribution to these features is beyond the scope of the current report. Future work will address this issue by extending the analysis to include the full ensemble of EC-Earth CMIP6 simulations produced by the consortium and investigating factors such as the relative skill of ensemble members (note from Figure 2.2 that r6i1p1f1 and r11i1p1f1 have an enhanced cold bias in the area of interest) and the uncertainty in projections of sea ice extent and SST.

3.2 Precipitation Projections

Figure 3.9 presents the spatial distribution of annual precipitation projections (% change) for each of the four SSPs for the 2041–2070 period. The corresponding projections for 2071–2100 are presented in Figure 3.10. The general trend is for an increase in precipitation except in the North Atlantic region south of Iceland and regions just north and south of the equator, including North Africa and large parts of South America and South Africa. Southern Europe and the Mediterranean show a drying for the end-of-century SSP3–7.0 and SSP5–8.5 projections. Note that the large projected changes over the Sahara and the Middle East should be considered in the context of small increases/decreases in precipitation in dry regions, resulting in large percentage changes (see Figures 2.12a and b for observed global precipitation data).

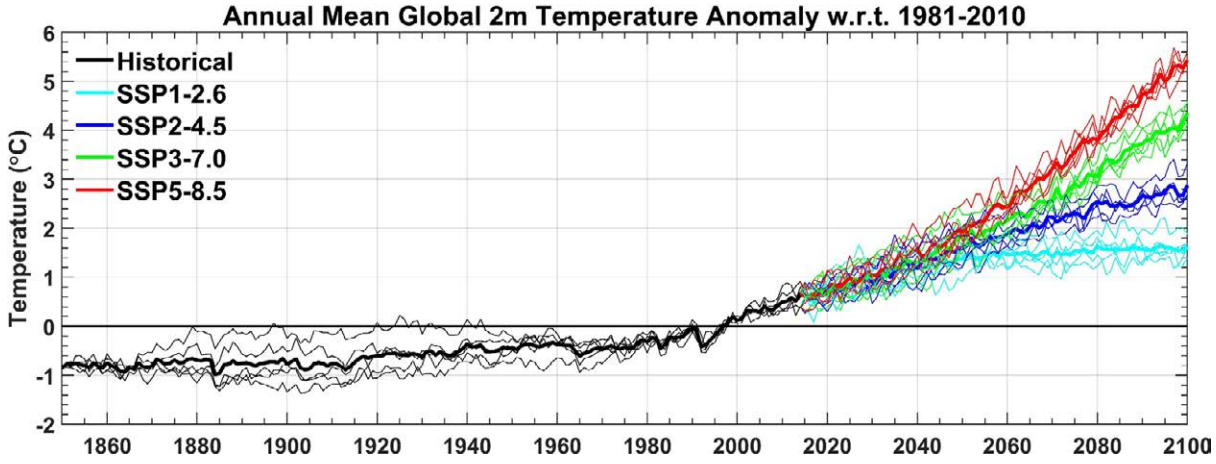

Figure 3.7. Global mean annual 2-m temperature anomalies with respect to the 30-year period 1981–2010: EC-Earth ensemble members r6i1p1f1, r9i1p1f1, r11i1p1f1, r13i1p1f1 and r15i1p1f1. The bold lines represent the ensemble means.

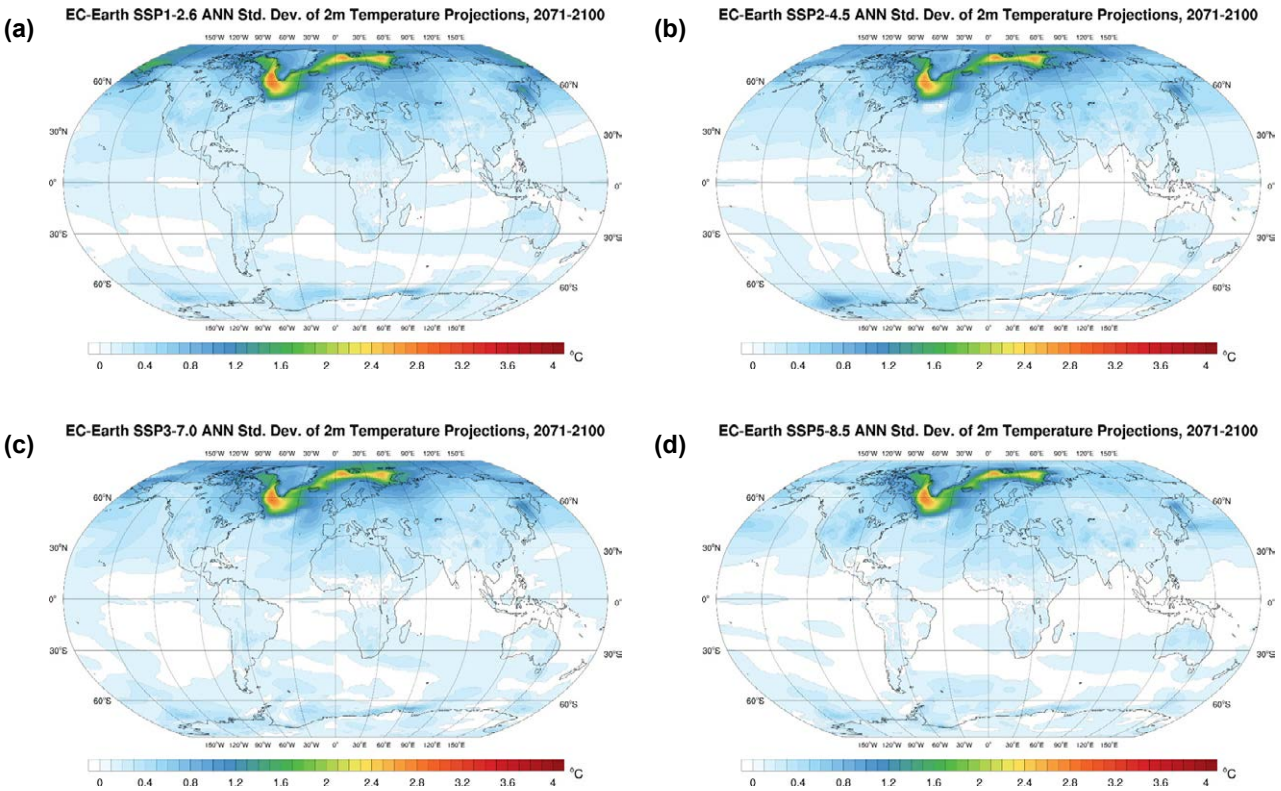

Figure 3.8. Standard deviation of the ensemble of annual 2-m temperature projections (2071–2100): (a) SSP1–2.6, (b) SSP2–4.5, (c) SSP3–7.0 and (d) SSP5–8.5.

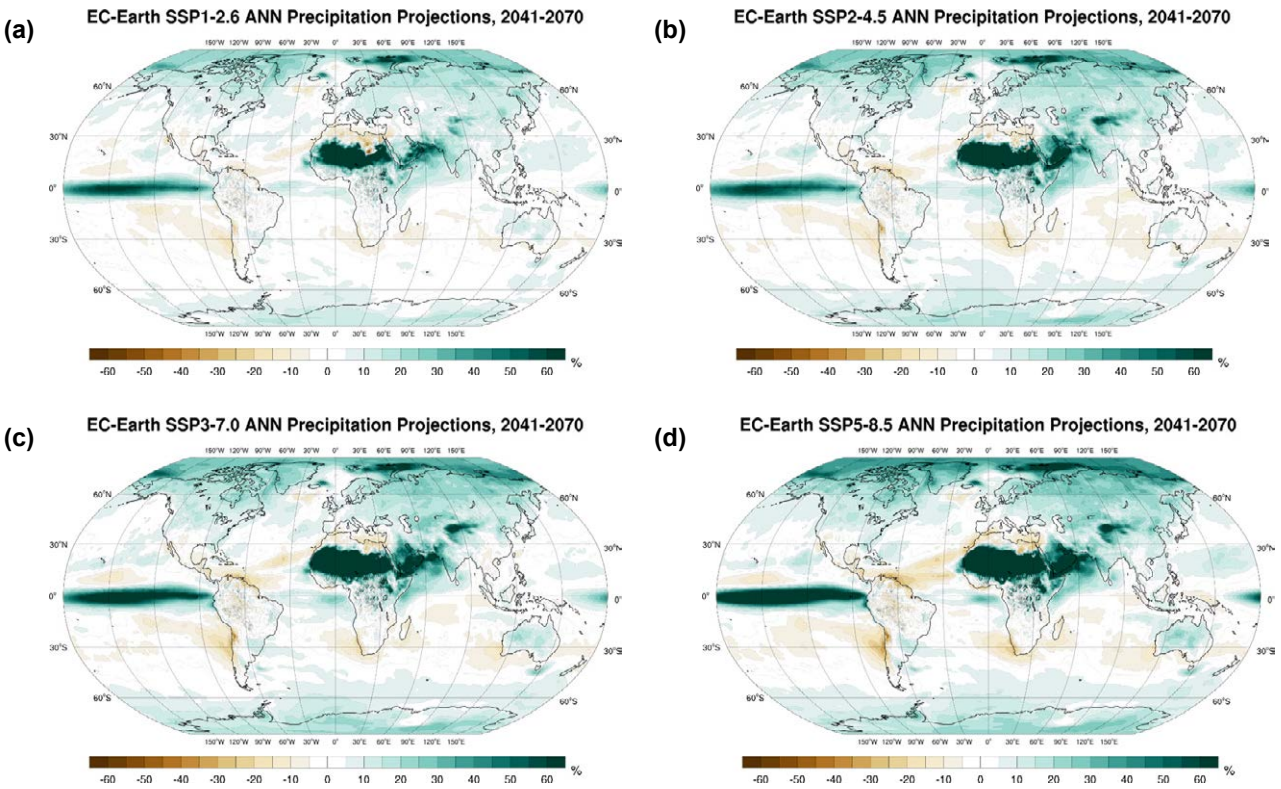

Figure 3.9. EC-Earth annual precipitation projections (2041–2070 vs 1981–2010, % change): (a) SSP1–2.6, (b) SSP2–4.5, (c) SSP3–7.0 and (d) SSP5–8.5. In each case, an average is taken of the ensemble members r6i1p1f1, r9i1p1f1, r11i1p1f1, r13i1p1f1 and r15i1p1f1.

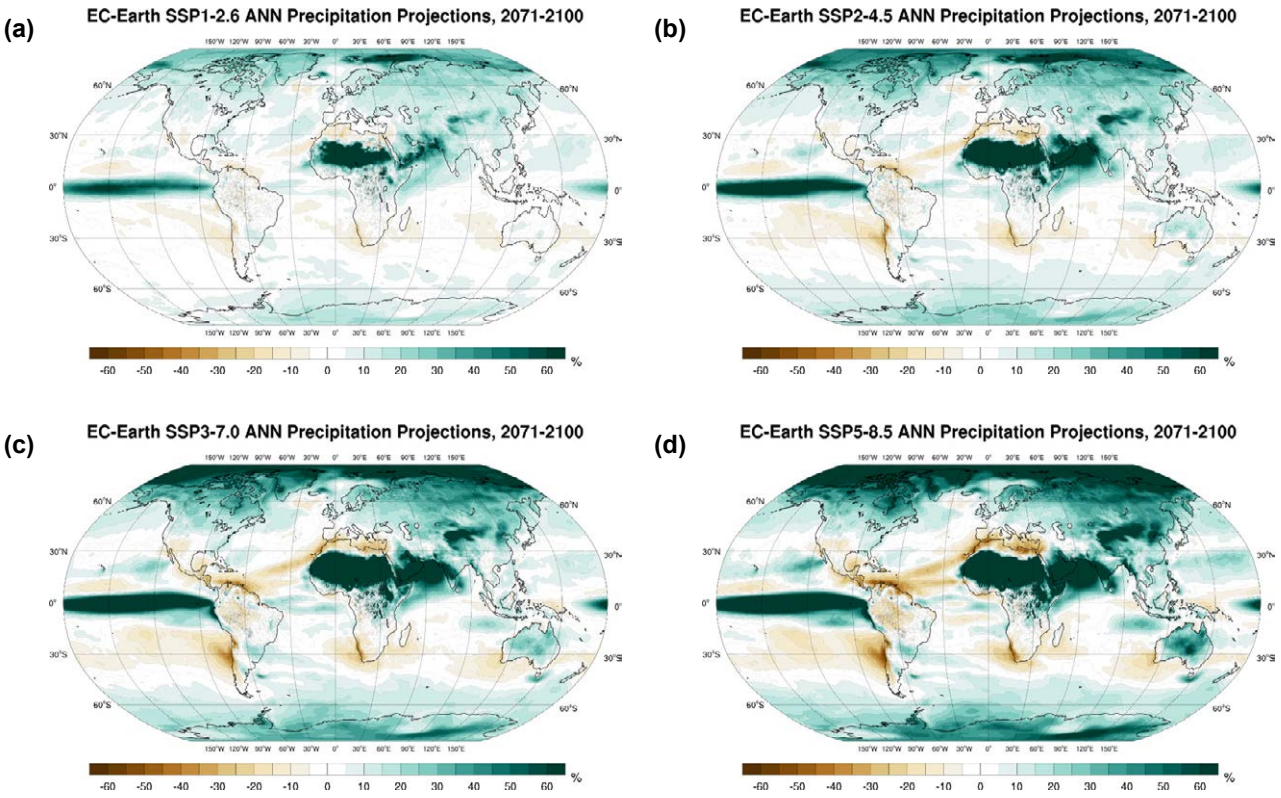

Figure 3.10. EC-Earth annual precipitation projections (2071–2100 vs 1981–2010, % change): (a) SSP1–2.6, (b) SSP2–4.5, (c) SSP3–7.0 and (d) SSP5–8.5. In each case, an average is taken of the ensemble members r6i1p1f1, r9i1p1f1, r11i1p1f1, r13i1p1f1 and r15i1p1f1.

Precipitation projections for DJF (Figures 3.11 and 3.12) follow a similar (but enhanced) trend to the annual projections. However, Europe and the Mediterranean are projected to be wetter under all SSPs. The projections for JJA (Figures 3.13 and 3.14) follow a similar trend to the annual projections, with a general increase in precipitation in most regions and an enhanced drying over southern Europe, North America, South America and South Africa. For JJA, there is no drying projected in the Atlantic region south of Iceland.

The mean global annual precipitation anomalies (relative to 1981–2010) for all five historical simulations (1850–2014) and 20 SSPs (2015–2100) are presented in Figure 3.15. The bold lines represent the ensemble means. All ensemble members show a steady increase in precipitation from around 2000, with a noticeable divergence between the SSPs around 2060. By the year 2100, global mean precipitation is projected to increase by approximately 4% (0.1 mm/day), 6% (0.16 mm/day), 8% (0.25 mm/day) and 10% (0.3 mm/day) for SSP1–2.6, SSP2–4.5, SSP3–7.0 and SSP5–8.5, respectively.

Compared with temperature (see Figure 3.7), the spread between ensemble members is enhanced for precipitation. However, the spread between ensemble members is greatly decreased compared with CMIP5 (Gleeson *et al.*, 2013), suggesting an added measure of confidence for the CMIP6 precipitation projections. Figure 3.16 shows the standard deviation of each SSP ensemble of climate projections; there is a high level of agreement between ensembles for most regions except North Africa and the Middle East (see note 6 regarding percentage changes in dry regions), the equatorial Pacific region and, to a lesser extent, over Australia and the Arctic.

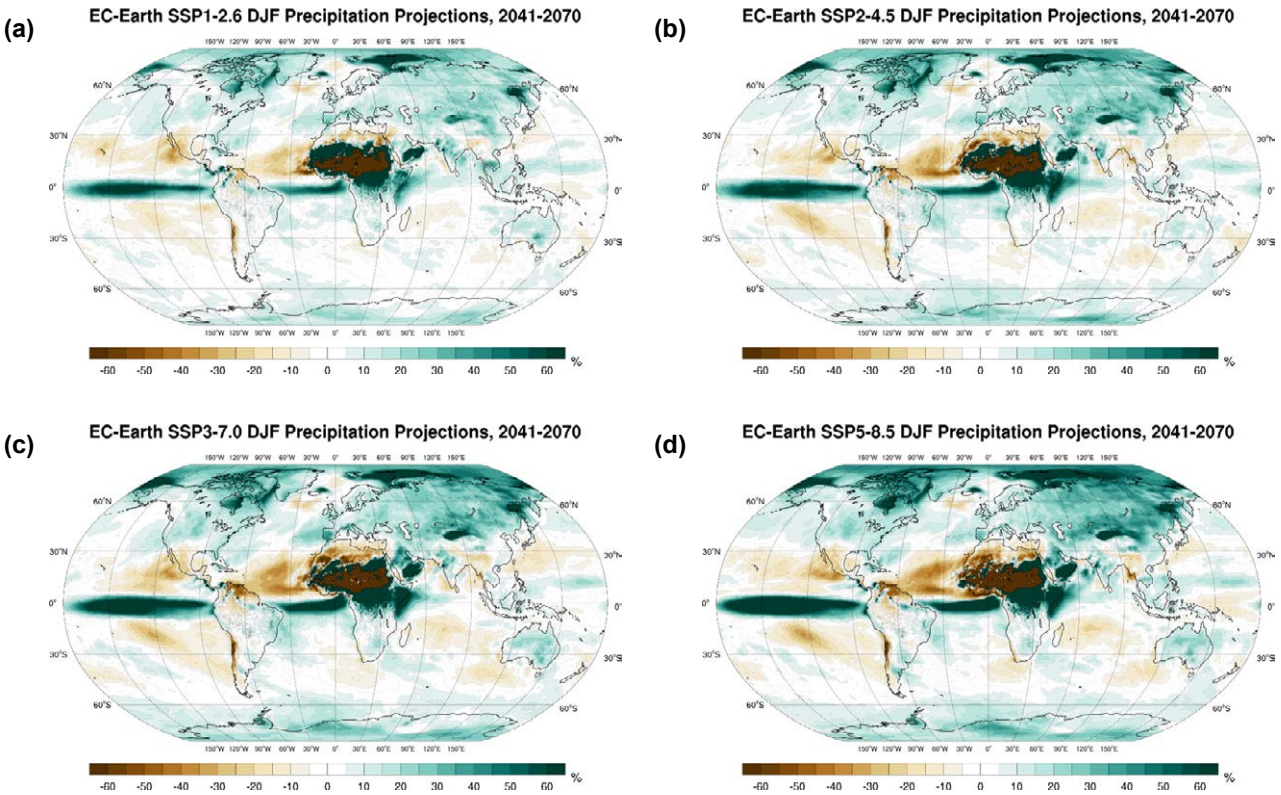

Figure 3.11. EC-Earth DJF precipitation projections (2041–2070 vs 1981–2010, % change): (a) SSP1–2.6, (b) SSP2–4.5, (c) SSP3–7.0 and (d) SSP5–8.5. In each case, an average is taken of the ensemble members r6i1p1f1, r9i1p1f1, r11i1p1f1, r13i1p1f1 and r15i1p1f1.

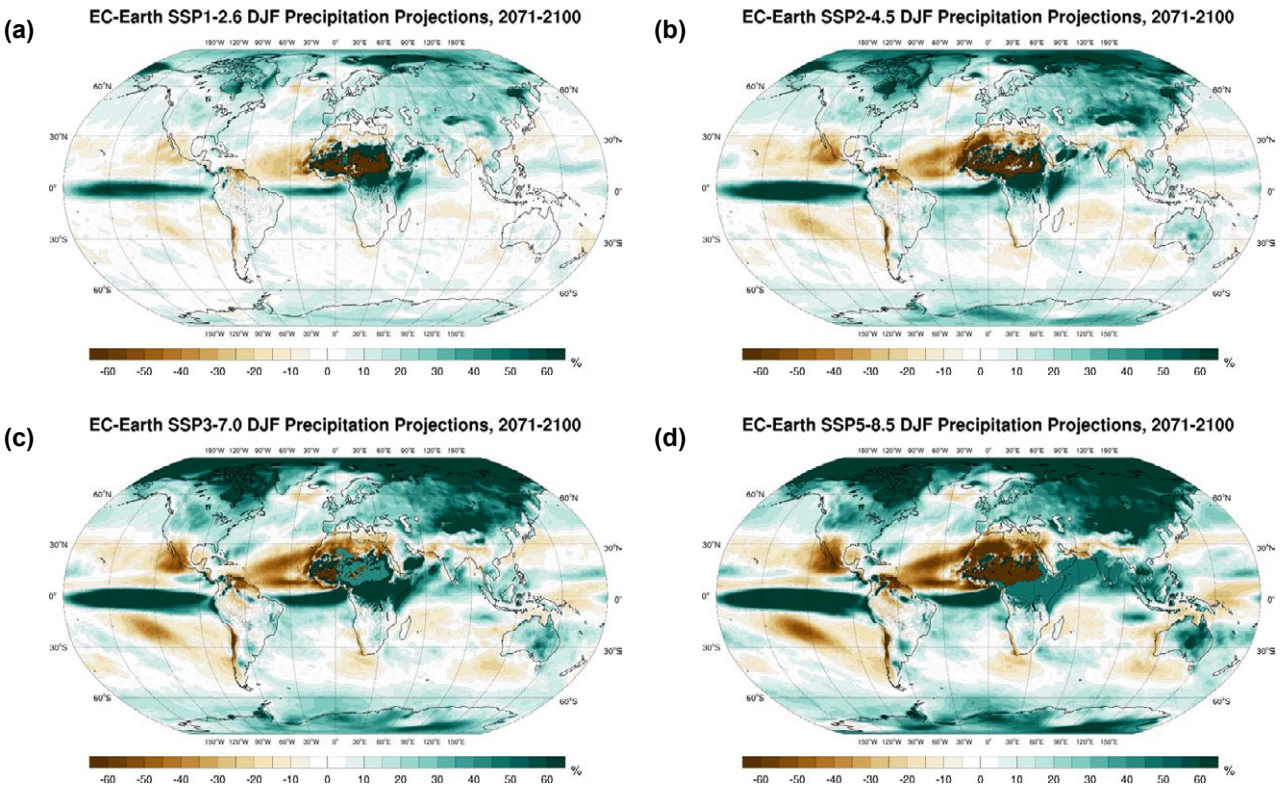

Figure 3.12. EC-Earth DJF precipitation projections (2071–2100 vs 1981–2010, % change): (a) SSP1–2.6, (b) SSP2–4.5, (c) SSP3–7.0 and (d) SSP5–8.5. In each case, an average is taken of the ensemble members r6i1p1f1, r9i1p1f1, r11i1p1f1, r13i1p1f1 and r15i1p1f1.

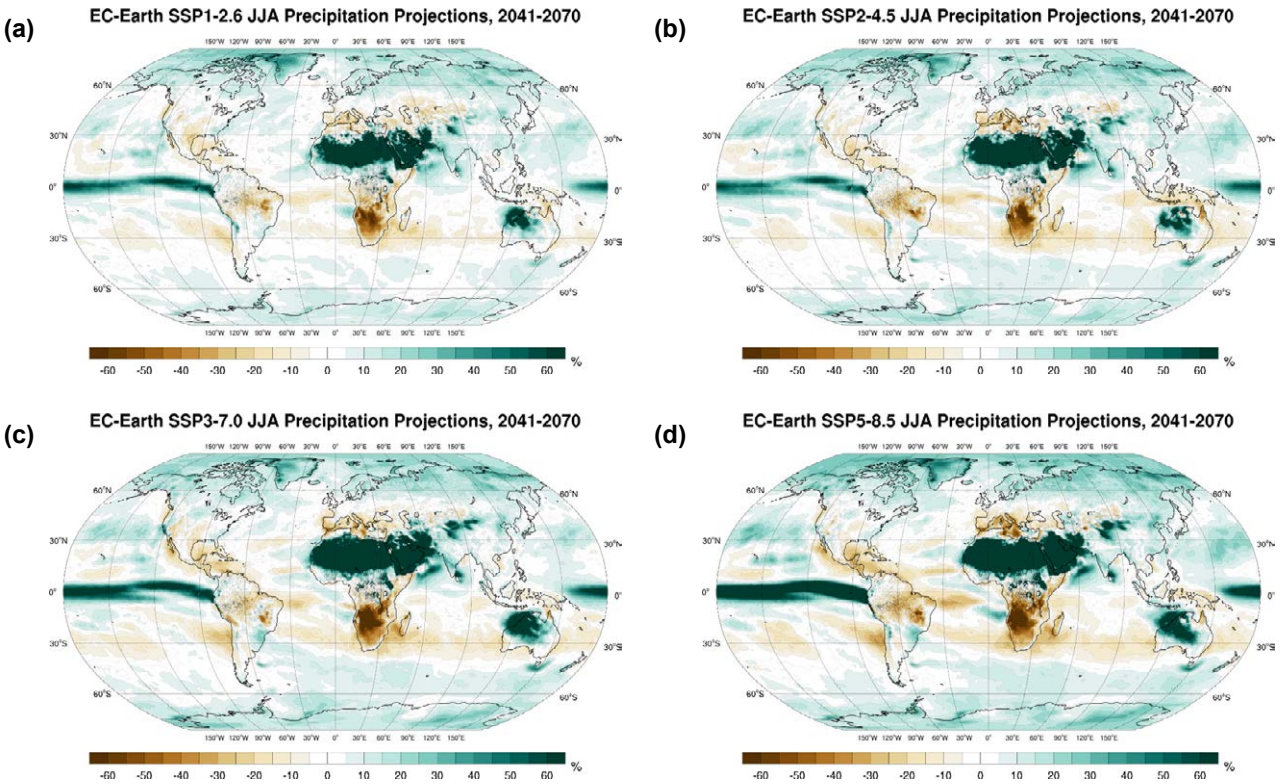

Figure 3.13. EC-Earth JJA precipitation projections (2041–2070 vs 1981–2010, % change): (a) SSP1–2.6, (b) SSP2–4.5, (c) SSP3–7.0 and (d) SSP5–8.5. In each case, an average is taken of the ensemble members r6i1p1f1, r9i1p1f1, r11i1p1f1, r13i1p1f1 and r15i1p1f1.

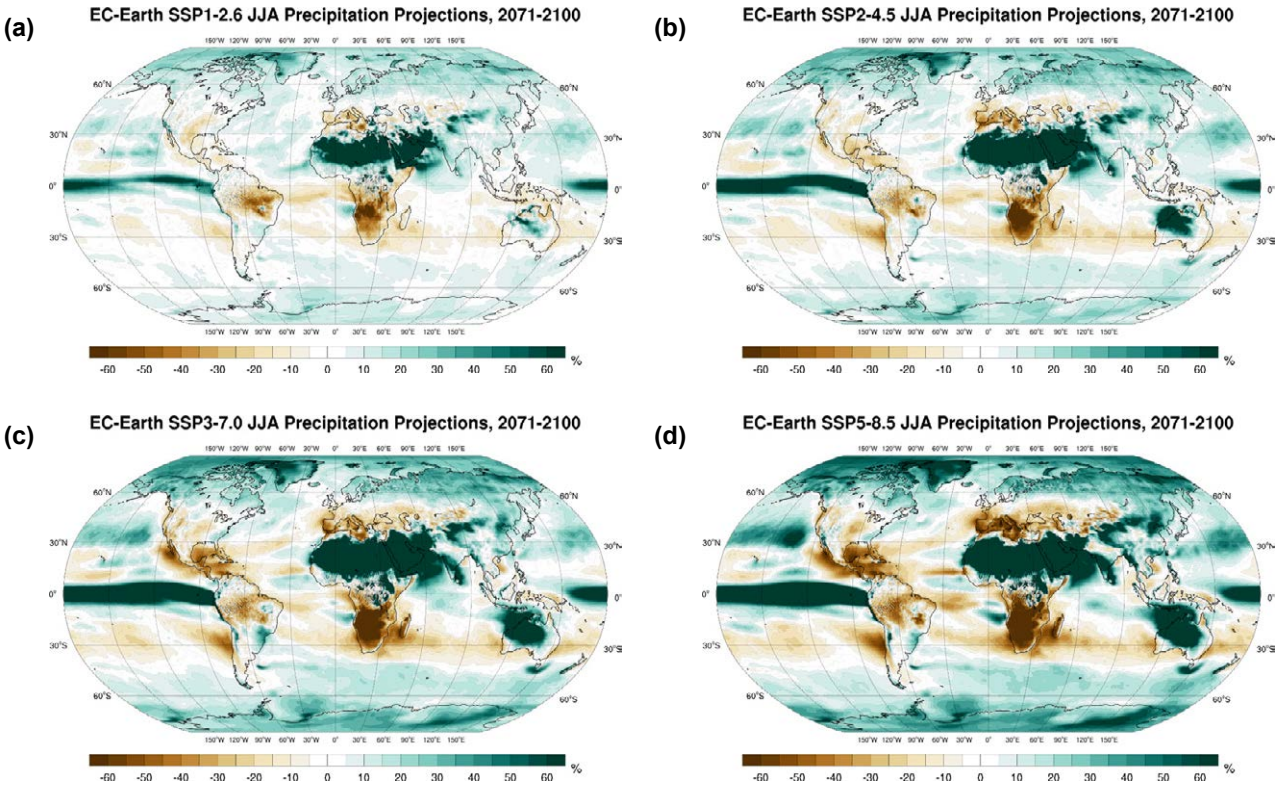

Figure 3.14. EC-Earth JJA precipitation projections (2071–2100 vs 1981–2010, % change): (a) SSP1–2.6, (b) SSP2–4.5, (c) SSP3–7.0 and (d) SSP5–8.5. In each case, an average is taken of the ensemble members r6i1p1f1, r9i1p1f1, r11i1p1f1, r13i1p1f1 and r15i1p1f1.

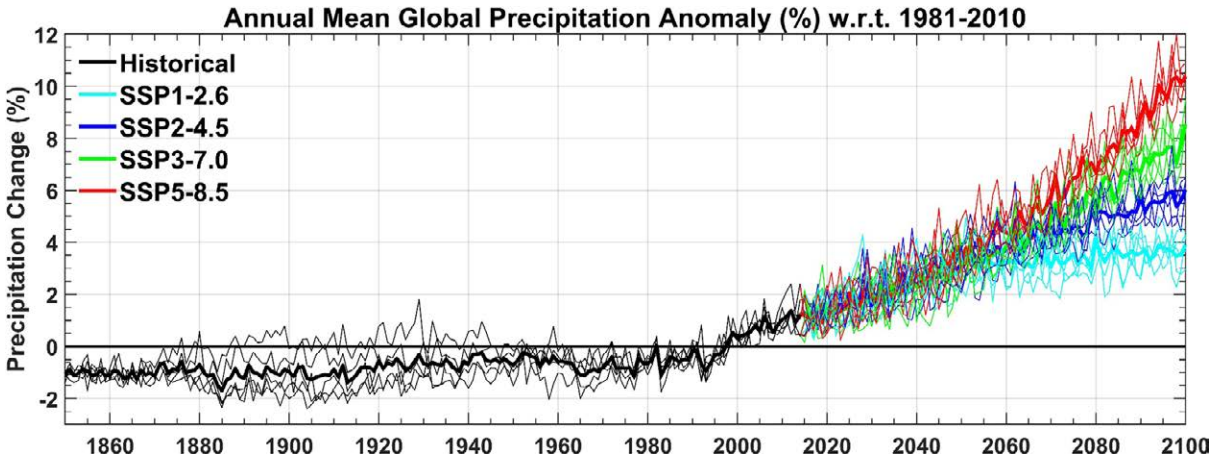

Figure 3.15. Global annual precipitation anomalies (%) with respect to the 30-year period 1981–2010: EC-Earth ensemble members r6i1p1f1, r9i1p1f1, r11i1p1f1, r13i1p1f1 and r15i1p1f1.The bold lines represent the ensemble means.

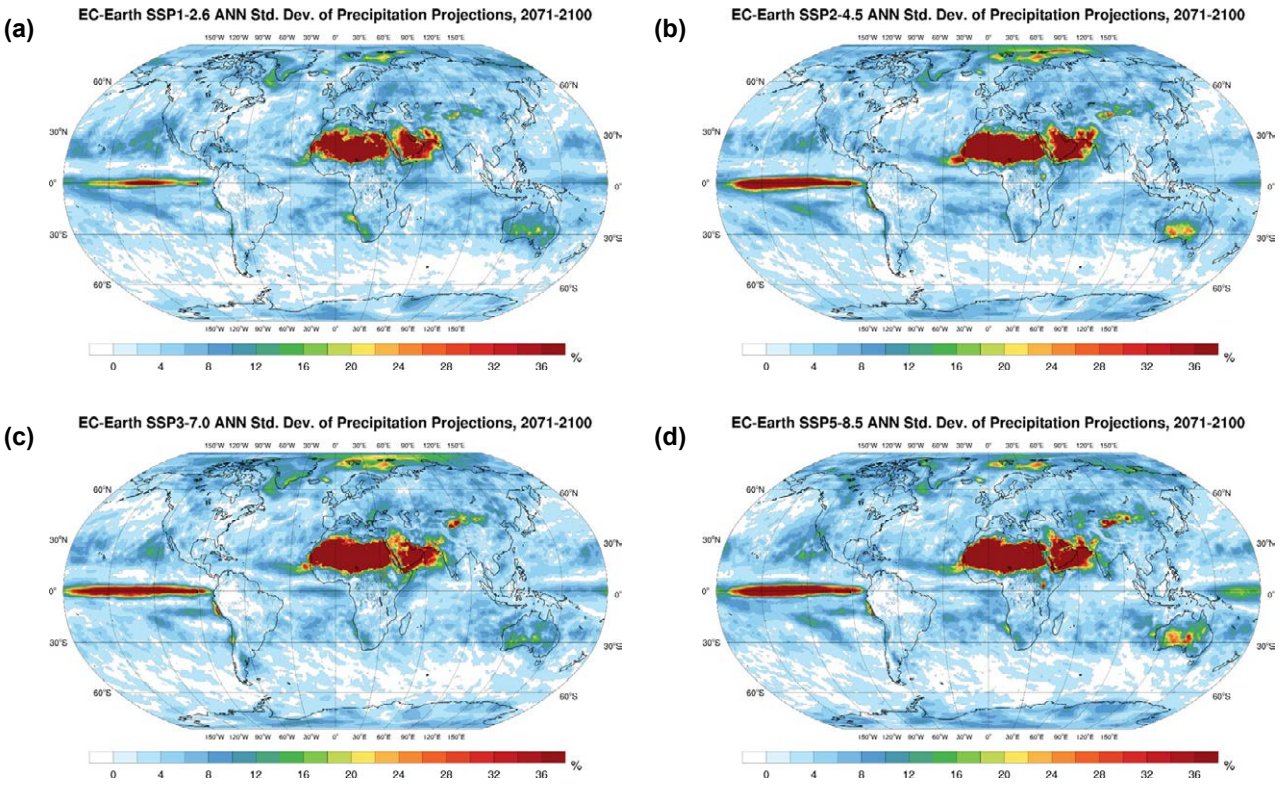

Figure 3.16. Standard deviation of the ensemble of annual precipitation projections (2071–2100): (a) SSP1–2.6, (b) SSP2–4.5, (c) SSP3–7.0 and (d) SSP5–8.5.